8-9-2014

A Three-Dimensional in Vitromodel of Atherogenesis

Pin Hsuan Chang
University of South Carolina - Columbia

A THREE-DIMENSIONAL *IN VITRO* MODEL OF ATHEROGENESIS

by

Pin Hsuan Chang

Bachelor of Science
National Taiwan University, 2013

Submitted in Partial Fulfillment of the Requirements

For the Degree of Master of Science in

Biomedical Engineering

College of Engineering and Computing

University of South Carolina

2014

Accepted by:

Richard L. Goodwin, Director of Thesis

Chandrashekhar V. Patel, Reader

Lacy Ford, Vice Provost and Dean of Graduate Studies

ACKNOWLEDGEMENTS

It took a great team for this work to be accomplished. First of all, I would like to thank my mentor Dr. Richard Goodwin, who picked me up when I was in the middle of nowhere, guided me with his profound knowledge, encouraged me with his endless patience and let me improvise because of his confidence in me. Without his unconditional support, I could never have made this far. Next, I would like to thank Dr. Daping Fan for the funding, valuable advice on experimental designs, and all the equipment I borrowed from his lab. I would like to thank Charity Fix and Lorain Junor, the two heroes who have taught me almost everything I know in cell culturing and all the other experimental techniques, and have helped me prepare all the necessary materials for this project. I would like to thank my lab mates Stefanie Biechler, Tzlil Perahia, Ashlie Evans Riley, Rebecca Jones and Katrina Harmon, who have helped me get off to a smooth start, inspired me in every possible way during the journey, and made sure that I landed firmly and carefreely. I would like to thank Dr. Shekhar Patel for always taking short notices from me; Dr. Robert Price, Dr. Jay Potts, Anna Harper, Jeff Davis, Benny Davidson and Sharon Cooper for their help in instrument resource facility; Dr. John Eberth for his advice in CFD modeling, and Mike Gore and Joey Farrow for the beautiful metal molds. Last but not least, I would like to say thank you to my mother, without whom I could have done nothing.

ABSTRACT

Atherosclerosis is the narrowing of arteries caused by accumulation of cholesterol, calcium and other cellular debris in the inner arterial wall. While extensive studies have been focusing on the inflammatory mechanisms of the disease, pathological and experimental evidence has shown that regions of disturbed flow are susceptible to the atherogenesis. To further understand the relationship between hemodynamics and atherogenesis, this research aims to generate a dynamic, 3D in vitro model of atherogenesis. This will allow for the investigation of specific cellular and molecular mechanisms of plaque formation that will pave the way for new therapies for the disease. A novel fabrication method that produces a 3D vascular construct was developed, which contains the cellular (endothelial cells, smooth muscle cells, and fibroblasts) and extracellular components of native vessels (type I collagen). Briefly, a combination of cells and solubilized collagen are polymerized in a tube mold to create the vascular tissue construct. The resulting tube, or the "cytotube", contains a radial-symmetric nozzle-like structure in the center of the construct, which was design to generate disturbed flow as fluid passes through the structure. CFD (computational fluid dynamics) modeling indicated an area of recirculating (disturbed) flow downstream the nozzle. Cell viability, morphology and protein expression in the cytotubes were investigated with confocal microscopy. These studies found that all fibroblasts, smooth muscle cells, and endothelial cells remained viable and have expressed various phenotypic morphologies in the cytotubes over 7 days of static culture. The proposed fabrication method and the resulting

model not only can serve as an in vitro 3D culture system and pathogenesis monitoring system, but also has the potential to influence vascular tissue-engineering studies.

TABLE OF CONTENTS

LIST OF FIGURES

CHAPTER 1
INTRODUCTION

1.1 Purpose of the Study

Atherosclerosis, a prelude to life-threatening cardiovascular diseases (CVD) such as stroke, aneurysm, myocardial infarction and many other coronary or peripheral arterial diseases, has been a companion of human species for thousands of years. [1]–[3] It is the hardening and narrowing of arteries caused by accumulation of cholesterol, lipids, calcium and other cellular debris in the inner arterial wall. Despite its prevalence, atherosclerosis has not come into the spotlight until the last century, when modern diet, life-style as well as modern medicine have gradually altered the spectrum of mortality. According to American Heart Association and World Health Organization, CVD itself has led to more than 30% of all deaths not only in the United States but worldwide since mid-1900s, among which nearly 80% were attributed to atherosclerosis-related conditions. [3]–[6] Throughout the last several decades, researchers have been mining for the underlying causes of atherogenesis, and it was only until the 1990s that the respond-to-injury hypothesis of the disease began supported by more data and then confirmed. [2], [7], [8] However, while the inflammatory mechanisms of the pathogenesis have drawn major attentions, pathological and experimental evidence has also shown that regions of complicated flow patterns in arteries, such as bifurcations, bends and junctions, are particularly prone to atherogenesis. [9]–[14] (Figure 1.1) Vast and growing studies have tried a variety of approaches – from animal experiments to cadaver specimens, from in

vivo analysis to in vitro observations. Nonetheless, in vivo investigations featuring living animals or human patients (CT or MRI scans) have intricate multicellular responses and individual physiological conditions, which complicates the analysis and interpretation fo collected information. Whereas, in vitro experiments using standard two-dimensional cell culture are too simplified to represent the in vivo tissue behaviors. Given the reasons, the main purpose of this study is to generate a three-dimensional arterial model in vitro that supports the cells of interest in a physiologically-relevant phenotype, while having the ability apply disturbed flow patterns to determine its role in atherogenesis.

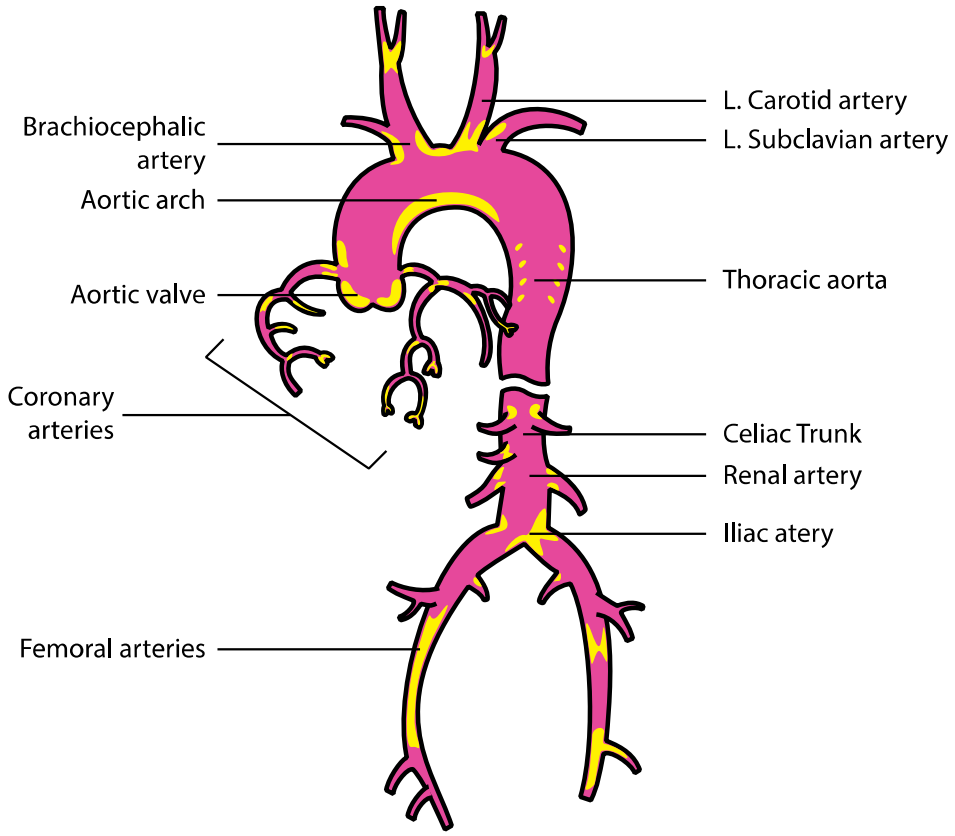

Figure 1.1 Common sites to find atherosclerosis. These sites include junctions, bends and bifurcations like coronary arteries, carotid arteries, iliac arteries, aortic valve and aortic arch. [14]

1.2 Structure of an Artery as Basis for Vascular Tissue Engineering

A typical arterial wall consists of three relatively distinct layers. From the lumen to the outer-most layer are tunica intima, tunica media and tunica adventitia (or tunica externa). The tunica intima is the thinnest layer and is composed of endothelium, basement membrane, lamina propria and a fenestrated layer of elastic fibers called the internal elastic laminae that separates the intima from media. The endothelial cells regulate anti-coagulation activities by secreting specific molecules like nitric oxide (NO), which inhibits platelet activation and prevents thrombogenesis. The basement membrane contains type IV collagen, laminin, and heparin that are associated with cell adhesion, migration, proliferation, phenotype and survival. [15][16]

The tunica media, which is the middlemost and the thickest layer of the three layers, consists of smooth muscle cells arranged circularly around the blood and a layer of external elastic laminae that separates the media from adventitia. In addition, tunica media contains variable proportion of interstitial matrix depending on the location, size and functionality of the artery. For large elastic arteries such as aorta and its largest branches including the brachiocephalic, common carotid, subclavian and iliac arteries, the tunica media is abundant in elastin arranging into concentric fenestrated lamellae separated by smooth muscle cell layers and collagen fibers. The elasticity and extensibility contributed by such arrangement allows the elastic arteries to withstand and regulate the rapid and vigorous fluctuation of blood flow proximal to the heart. [17] In contrast, smaller muscular arteries contain layers of smooth muscle cells, from as few as 3~5 layers to as many as 25~40 layers. Muscular arteries also contain ECM within media, but with relatively more collagen (type I and type III) than elastin fibers and the

laminated architecture of the elastin lamellae are hardly present. [18], [19] Under physiological conditions, the quiescent contractile smooth muscle cells within muscular arteries control vasoconstriction and vasodilation to regulate blood flow and pressure. Under pathological conditions however, different cell types including ECs, platelets and inflammatory cells release mediators that convert smooth muscle cells into an active synthetic and non-contractile phenotype, which lead to cell proliferation, migration and increased extracellular matrix production. [20] It is important to note that the mechanisms that regulate this process are not well understood.

The tunica adventitia is composed of collagenous connective tissue that varies from higher density near the tunica media to lower density that merges with the connective tissue surrounding the blood vessel. [21] The collagen fibers are primarily type I collagen, which in adventitia the collagen forms two helically arranged families of fibers. Collagen fibers play a significant role in stability and strength of the arterial wall. In unstressed condition, collagen fibers are embedded in a wavy form, causing adventitia to be softer than media. However, when a significant level of strain is applied, collagen fibers reach their straightened lengths and the mechanical response of adventitia then changes to that of a stiffer material, preventing the artery from overstretch and rupture. [19][22] Besides extracellular matrix, adventitia contains fibroblasts and other inflammatory cells like macrophages that participate in immune response to foreign antigens and arterial injuries [23][24], as well as nerve tissues and vasa vasorum, or microvessels of blood vessel, that mediate and nourish the medial smooth muscles. Figure 1.2 shows the layered structure of an artery.

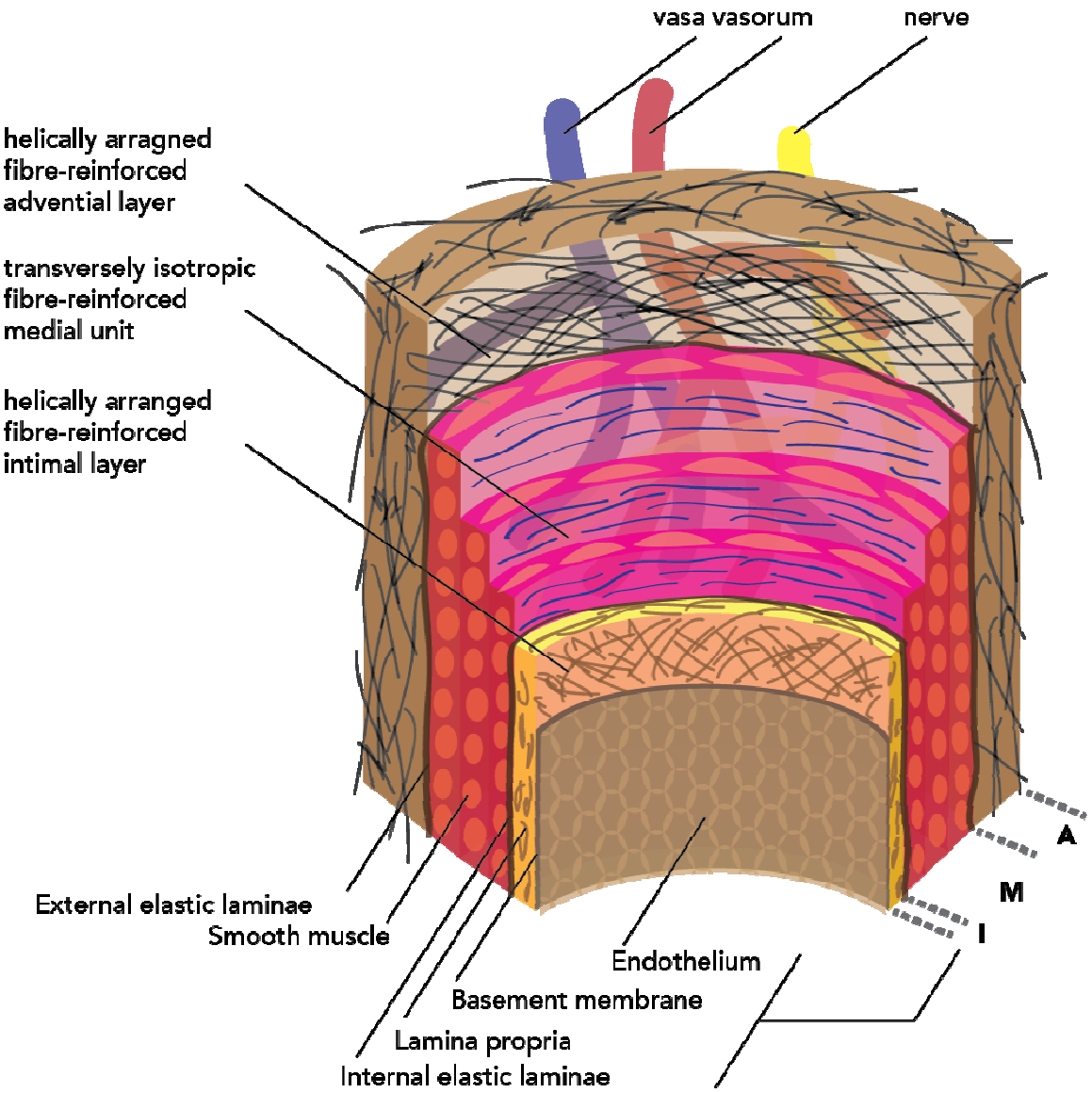

Figure 1.2 The layered structure of an artery. From lumen to outer wall are tunica intima (I), tunica media (M) and tunica adventitia (A).

1.3 Collagen as a Scaffold Material in Vascular Tissue Engineering

Since 1986 when Weinberg and Bell [25] reported a type I collagen based in vitro blood vessel model, type I collagen hydrogels have been explored for use in vascular tissue engineering. [26] Type I collagen is the most abundant type of collagen in adult

connective tissues such as skin, bone and tendon. A mammalian type I collagen molecule has a triple-helix structure composes of two α1(I) chains and one α2(I) chain. In vivo, these molecules form intermolecular cross-links and wrap into fibrils, contributing to the integrity and mechanical strength of the tissues. [27] When solubilized with protease (pepsin) or acids; however, the intermolecular cross-links are broken down, allowing for the collagen to become soluble. Particularly, collagen derived by pepsin digestion is high in purity and low in antigenicity, thanks to the telopeptide-specific cleavage by pepsin, which removes most potential antigens. [28], [29] Collagen extracted by such methods is soluble in acidic environment between pH 1 ~ pH 4, and when neutralize, this collagen can then undergo an aldehyde condensation reaction that reforms the intermolecular cross-links, which makes it a very plastic scaffold biomaterial.

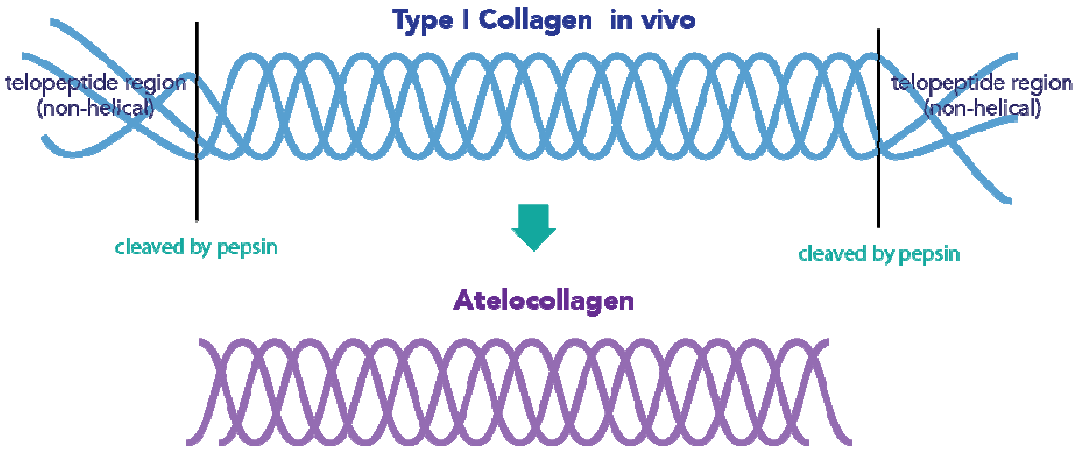

Figure 1.3 Type I collagen extraction with pepsin allows for exclusion of non-collagen proteins that may be antigenic, which increases the biocompatibility of the material.

1.4 Experimental Approach

The in vitro arterial model for atherogenesis contains a constriction nozzle in the middle of the tube (Figure 1.4), so that when fluid (media) passes through the

constriction, a disturbed flow pattern is generated. Computational fluid dynamics (CFD) modeling was applied in this study to help visualize and predict fluid behavior in the proposed model.

For the scaffold material, we have chosen bovine type-I collagen for its biocompatibility and plasticity. For cellular components, we will use rat aortic smooth muscle cells (RASMC) to generate the muscular tunica media, and rat aortic endothelial cells (RAEC) to form the monolayer endothelium. ECs and SMCs have the most immediate association with the onset of atherogenesis, and a variety of cytokines induced by corresponding levels of flow shear stress within these two cell types has been thought to be the culprit of the disease. This proposed 3D model will serve as a tool to observe cell-cell, cell-ECM and cell-flow interactions. Preliminary optimization experiments were first tested on rat heart fibroblasts (AHF) and individual cell types, which will also give us the information of the differences between single and co-cultured systems.

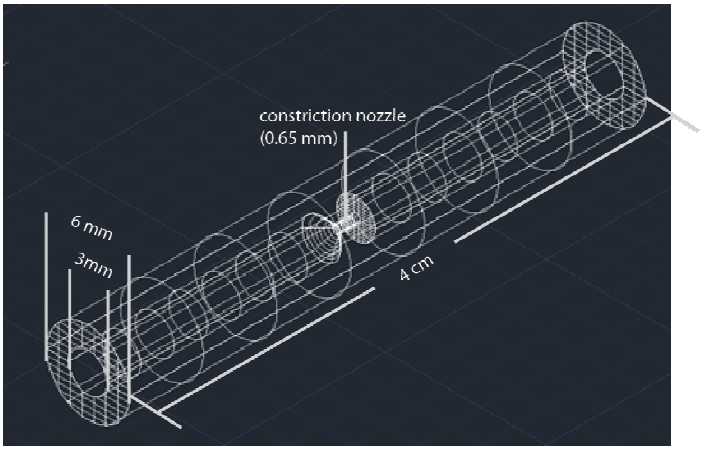

Figure 1.4 The geometry of the proposed in vitro arterial model. The model contains a constriction nozzle in the middle of the tube, so a disturbed flow pattern is expected to be generated when flow passes through the nozzle. The fluid dynamics in the model will be analyzed with computational fluid dynamics modeling software to confirm this assumption and model the cahracteristics of flow through the tubular construct.

CHAPTER 2
MATERIALS AND METHODS

2.1 Computational Fluid Dynamics (CFD) Modeling

Fluid behavior passing through the proposed model was simulated with CFD software COMSOL Multyphysics® using finite element analysis (FEA) technique. Naiver-Stokes equations and continuity equations were adopted to reconstruct the velocity field, shear rate, streamline, pressure and particle. To validate and simplify, the computational analysis, several assumptions had been made. Firstly, the wall of the model was assumed to be rigid, therefore any forces caused by the movement or deformation of the wall could be neglected. Secondly, the heterogeneous surface between the fluid and the inner wall of the tube was assumed to be non-slip, leading to the boundary condition $u_{wall} = 0$, where u_{wall} is the fluid velocity at the wall. Thirdly, the input fluid was chosen to be water, hence was assumed to be Newtonian and incompressible with density of 9.93×10^{2} kg/m^3 and viscosity of 6.92×10^{-4} Pa·s at 37ºC. [30] Also, the input flow was fully developed steady flow at the entrance. Finally, the gravitational force was neglected so that the force field was regarded as axisymmetric along x-axis. Figure 2.1A shows the geometry of the model, and the flow would move along positive x-axis. The flow velocity profile was as follow:

$$2\left(1-\left(\frac{y^2+z^2}{R^2}\right)\right)\times u_{mean}$$

Where R is the inner radius of the channel and u_{mean} is the mean velocity of the flow. In this analysis, input flows of mean velocity 0.5 cm/s, 1.0 cm/s and 2.0 cm/s were simulated.

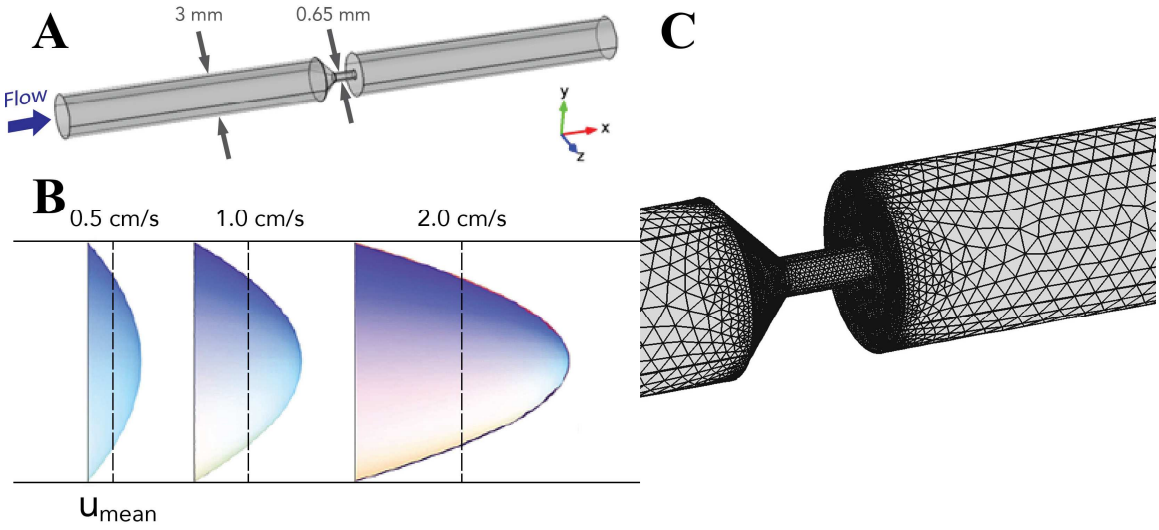

Figure 2.1 (A) The geometry of the modeled channel and flow direction (B) Velocity profiles of the input flow at different mean velocities. (C) Finite element analysis requires the modeled region be divided into fine meshes so that the computation is executed in each small compartment and then assembled into one complete result.

2.2 Cytotube Fabrication

2.2.1 Cell Culture and Cellular Suspension

Primary male adult heart fibroblast cells (AHF), rat aortic smooth muscle cells (RASMC) and aortic endothelial cells (RAEC) were grown in 10 mL DMEM (Dulbecco's Modified Eagle Medium) containing 10% fetal bovine serum (FBS), 1% Pennicilin/Streptomycin and 0.1% amphotericin B at 37°C, 5% CO_2 in 100 mm petri dishes. The media was changed every other day. Confluent cell plates of passage 6~12 were used in the following experiments.

To prepare cellular suspension for seeding, confluent plates of cells were trypsinized (0.25% Trypsin/0.1% EDTA), spun down and resuspended in fresh DMEM media. The concentration of the cellular suspensions was calculated using a hemocytometer (Bright-Line™, Sigma-Aldrich). At confluency, a 100 mm petri dish contains about 6×10^6 RASMC, 10×10^6 RAEC and 7×10^6 AHF. In this research, 1/2 plate of RASMC, RAEC or AHF were seeded in a cytotube, i.e. $2\sim3\times10^6$ RASMC, $4\sim5\times10^6$ RAEC and AHF.

2.2.2 Collagen Gel Preparation

The solubilized bovine type I collagen was obtained from the laboratory of DR. Mike Yost. The preparation method of bovine type I collagen was described in detail in Yost et al., 2004. [31] Briefly, the hide of an 18-month-old bovine steer was cut into strips and washed with deionized water. The remaining follicles and non-collagenous proteins were removed by treating in $Ca(OH)_2$ solution overnight. The next day, the strips were washed with DI water, placed in NaCl solution and neutralized with HCl to pH 6.8-7.0. The strips were then cut into smaller pieces and placed in acetic acid with pepsin overnight at 4ºC. Subsequently, the strips were emulsified into a gel dispersion using a food processor, from which the type I collagen was precipitated by adding a final concentration of 2M NaCl and neutralized to pH 7.2 with NaOH. The collagen precipitate was collected by centrifugation, and was resuspended in DI water followed by 2 days of dialysis versus DI water to remove excessive salt content. The resulting collagen gel was then centrifuged to rid excessive water and the pH value was adjusted to pH 2.5-3.0 with concentrated HCl solution.

Concentration calculations and pH value measurements were performed on the received collagen gel, which was stored in ten 50 mL conical tubes at 4ºC. For concentration test, 1~2 g collagen gel was extracted from each conical tube and was incubated at 100ºC overnight. The wet weight and dry weight of each collagen sample were both recorded for weight concentration calculation:

$$collagen\ gel\ w/w\% = \frac{dry\ weight\ (solute\ only)}{wet\ weight\ (solution)} \times 100\%$$

Meanwhile, the pH value of the collagen gel was tested for each conical tube using a pH meter (Accumet™ AB15 Basic, Fisher Scientific™). The received collagen gel had an average of 0.67±0.06 w/w% at pH 5.12±0.02. Figure 2.2A shows the result of using this concentration of collagen for making the tubular scaffold. Unfortunately, this concentration was too low for the resulting tubes to maintain their structure after polymerization in pH 7.4 HEPES buffer. To increase the concentration, the collagen gel was further centrifuged in filtered conical tubes (Amicon® Ultra-15 30K device, Millipore) at 2000 g, 4°C (RT6000B with H1000B Swinging Bucket Rotor, Sorvall®) to remove a portion of water content. Figure 2.2 shows that when the initial collagen concentration was ~1%, the integrity of the resulting tubes had observable improvement. After two 20-minute centrifugations, the volume of the gel was reduced by 50%~60% and the concentration of the gel was able to increase to 1.8±0.2 w/w% (3 N) and was used in the following experiments. Prior to each fabrication session, the condensed collagen gel was sterilized with 1200 rad γ-irradiation. During the entire fabrication procedure, the collagen gel was kept on ice to reduce polymerization initiated by increased temperature.

Figure 2.2 Integrity of the resulting collagen tubes made with different starting concentration. The collagen tubes made with the un-condensed collagen gel (~0.67%) were not able to maintain desired shape in vitro (A), while the tubes made with more condensed collagen gel (~1%) had observable improvement in maintaining integrity (B). A final concentration of ~1.8% collagen gel was used in the following fabrication procedure (C).

2.2.3 Optimizing Cell Survival in Collagen Gel

One of the major concerns of cell embedding in solubilized collagen is that the pH value and osmotic concentration of solubilized collagen gel may not be suitable for cells to survive. Thus, creating a similar environment between culture media and collagen gel before embedding the cells became a major challenge in this study.

HEPES buffer (10 mM HEPES, 0.14 M NaCl, 4.7 mM KCl, 1.3 mM $MgSO_4$, 1.6 mM $CaCl_2$), a widely used supplement in DMEM to maintain physiological pH value, was chosen as the neutralizing reagent for the solubilized collagen gel. Ideal final pH value of the neutralized collagen would be pH 7.4 for cell embedding procedure. To find the most suitable alkalinity of the neutralizing reagent, a series of 10X HEPES buffer with pH value ranging from 7.4 to 8.0 at 0.1 increments were added respectively to the solubilized collagen at 1:8 volumetric ratio (100 µL 10X HEPES : 800 µL solubilized collagen) and the pH values were measured again after mixing thoroughly. The

remaining one portion was reserved for cellular suspension. Figure 2.3 shows the adding sequence and proportion of solubilized collagen, neutralizing buffer and cell suspension.

Since each batch of condensed collagen gel had slightly different acidity, at least three batches of condensed collagen were tested to establish a look-up table. To optimize osmotic pressure for cell survival, dialysis tubing with large molecular weight cut-off (Spectra/Por® 2, MWCO 12-14 kDa, Spectrum) was chosen to ensure rapid small molecule exchanges such as water, salt, amino acids and other electrolytes while retaining large collagenous molecules within the tubing.

Figure 2.3 Collagen, neutralizing buffer and cell suspension proportions.

2.2.4 Mold Preparation

Figure 2.4 shows the metal molds custom-made in the machine shop (School of Medicine, University of South Carolina). Dialysis tubing of 10 mm flat width was cut into 5 cm pieces lengthwise, which will be called “sheaths” in the following description. Prior to use, the sheaths were submerged in pH 7.4 HEPES buffer in a conical tube to soften the material and were sterilized with 1200 rad γ-irradiation. The metal molds were autoclaved before use.

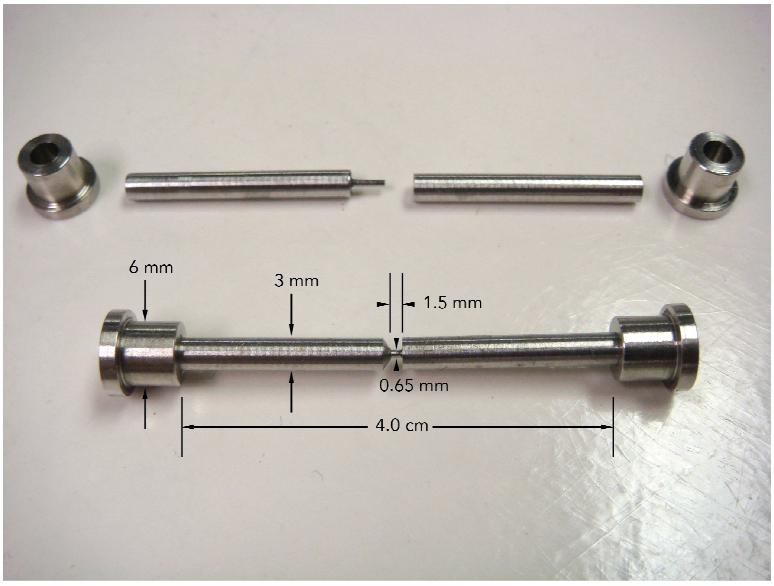

Figure 2.4 Specifications of the metal molds. Each set of mold consists of 2 caps and 2 central mandrels. The mold will generate a collagen tube of 3 mm inner diameter, 6 mm outer diameter and a constriction nozzle in the middle of 0.65 mm inner diameter.

2.2.5 Cytotube Fabrication I – Creating the Muscular Wall

In a sterile hood, the two rods and one cap of each set of the metal molds were assembled first. Next, the flat dialysis tubing sheaths were opened into cylinders and slipped on to the rim of the cap from the uncapped end of the mold. To make cellular collagen gel mixture, 1 mL collagen gel was loaded into a 1.5 mL microcentrifuge tube using a 1.0 mL syringe and was quickly mixed with 125 μL filter-sterilized 10X HEPES buffer to bring up the pH value of the gel to pH 7.4. Immediately after pH adjusting, 125 μL of AHF or RASMC suspension ($2\sim3\times10^7$ cells/mL) was added to the neutralized collagen gel and mixed thoroughly. The microcentrifuge tube containing the cell/collagen mixture was then centrifuged in a mini microcentrifuge for 5~10 seconds to remove air bubbles. Afterwards, mixture was slowly syringed into the molds and capped. Each set of mold was incubated at 37°C, 5% CO_2 in a sterile plastic culture tube (17×125 mm,

Fisherbrand™) in DMEM for 24 hours to allow for collagen polymerization. (Figure 2.5 A)

2.2.6 Cytotube Fabrication II – Creating Endothelium

The next day, the cytotubes were pulled out from the molds and transferred into new plastic culture tubes containing fresh media. 100 μL of RAEC suspension ($2\sim3\times10^7$ cells/mL) was pipetted into the lower half of the cytotube from the nozzle constriction, followed by another 100 μL cellular suspension being pipetted into the upper half of the cytotube. The culture tubes were then fastened onto a tube rotator (099A RD5512, Glas-Col®) and let rotate at the lowest speed (~17 rpm) at 37ºC, 5% CO_2 for 24 hours. The axial direction of the cytotubes was horizontal, aligning with the rotational axis of the rotator (Figure 2.5 B).

2.2.7 Cytotube Fabrication III – Static Culture

After RASMC, RAEC or AHF were seeded, each cytotube was transferred into a 60 mm petri dish and was cultured in DMEM at 37ºC, 5% CO_2 (Figure 2.5 C). The culture media was changed daily until the cytotubes were harvested for confocal imaging or qRT-PCR analysis. Meanwhile, the appearance of the cytotubes was recorded daily using a digital camera (T-100, Sony), and the dimensional changes through out the time were measured using ImageJ software.

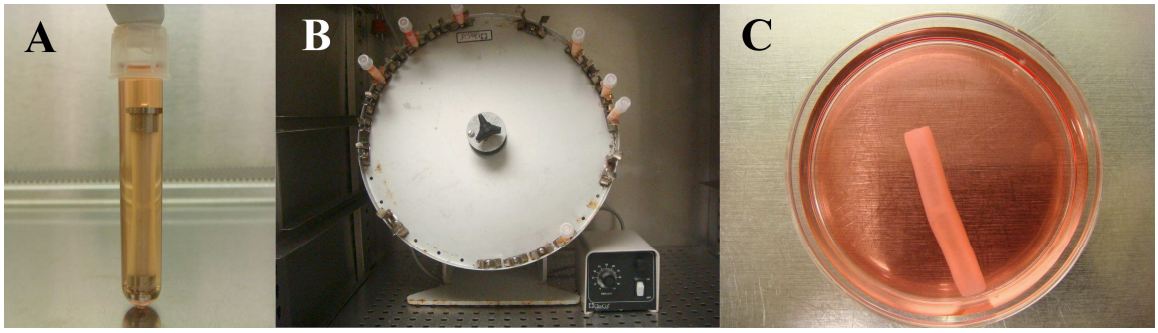

Figure 2.5 Cytotube culturing procedure. (A) The SMC/collagen set was let polymerize in a sterile test tube for 24 hours at 37°C, 5% CO_2. (B) The next day, polymerized cytotubes were removed from the mold, transferred into a new tube with fresh media, seeded with ECs within the lumen, and fastened horizontally onto a rotator for another 24 hours incubation. This step was necessary to evenly distribute cells inside the lumen. (C) After both SMCs and ECs were seeded (48 hours), the cytotubes were transferred into 60 mm petri dishes for several days more of static culture. Finally, the cytotubes were collected and prepared for confocal microscopy or other applications at certain time points.

2.2.8 Preparing for Confocal Microscopy

Cytotubes were grown for specific time points and then fixed in 4% paraformaldehyde (PFA)/phosphate buffer saline (PBS) at 4°C for at least one day. Next, the cytotubes were embedded in 5% agarose/PBS gel and sectioned longitudinally on vibratome (Oxford®) at 200 μm. The sections were treated with 0.25%Triton X-100/PBS for 20 minutes and washed with PBS for three times, followed by blocking with 2% bovine serum albumin (BSA)/PBS for 1 hour at room temperature.

Two different combinations of immunofluorescent labeling were used to identify and distinguish certain cell types. For cytotubes with single cell type, sections were stained with fluorescently labeled phalloidin (F-actin stain, Alex Flour 488®, Life Technologies™), 4'6-diamidino-2-phenylindole (DAPI, nuclear stain) and Cy3-labeld anti-alpha smooth muscle actin (Cy3-anti-αSMA, Sigma-Aldrich®). For cytotubes with both EC and SMC, sections were stained with FITC-labeled anti-von Willebrand factor

antibody (Abcam), Cy3-anti-αSMA, and DAPI overnight at 4°C. The sections were rinsed with 3 changes of PBS, each of which lasted 10 minutes, and were mounted on glass slides with 1,4- diazabicyclo[2.2.2]octane (DABCO) for confocal microscopy imagine (Zeiss LSM 510 Meta, Carl Zeiss).

2.2.9 Summary

The following is the summary flowchart of the fabrication method. Figure 2.6 displays the fabrication procedure with detailed illustrations.

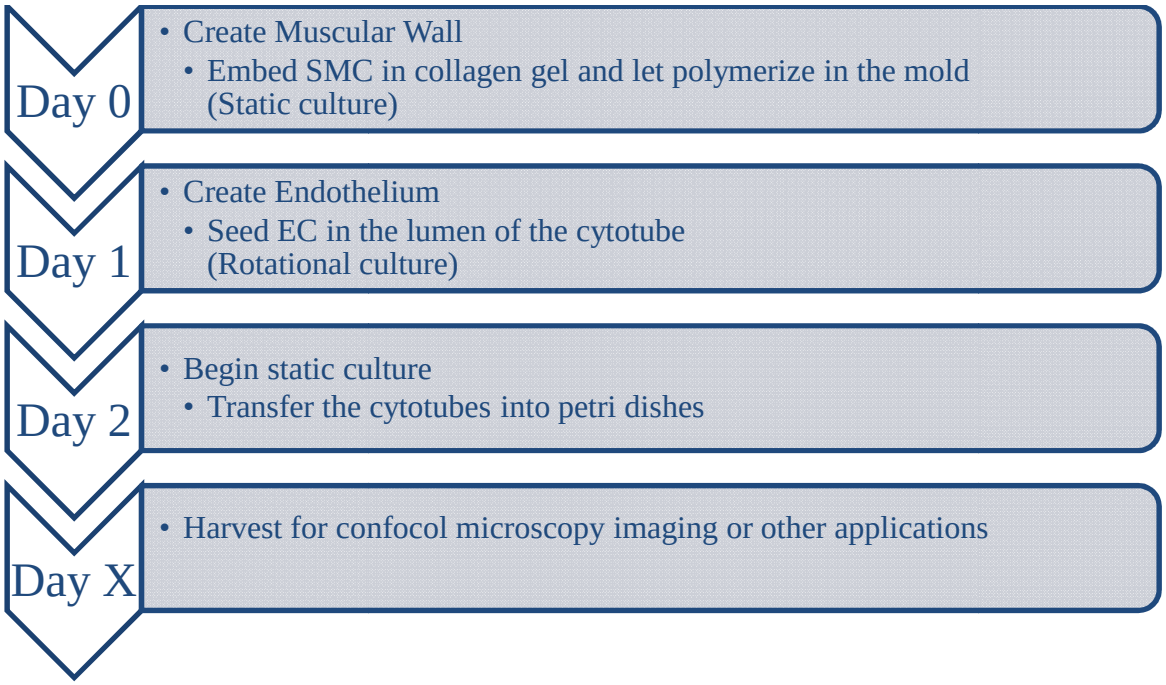

CYTOTUBE FABRICATION PROCEDURE

A. Collagen Condensation

Transfer dilute collagen to Millipore tube
(MWCO = 30 kDa)

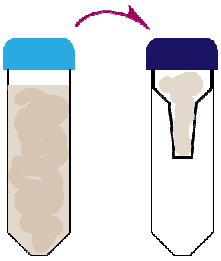

0.7% Collagen Gel

1. Centrifuge at 3000 rpm for 20 minutes.
2. Stir to redistribute concentration.
3. Centrifuge at 3000 rpm for another 20 min.

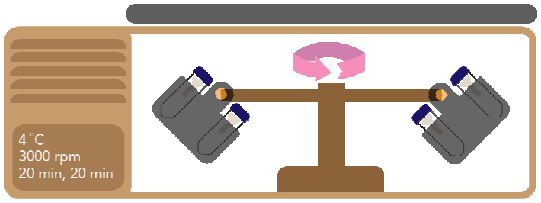

When the volume
reduced 50%~60%

Collect the concetrated collagenand
sterilize with 1200 rad gamma-irradiation

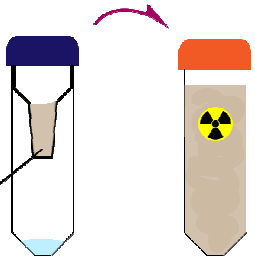

1.8%~2.0%
Collagen Gel

B. Creating Muscular Wall (Day 0)

Transfer 1.0 mL collagen
into a microcentrifuge tube
with 1.0 mL syringe (no needle)

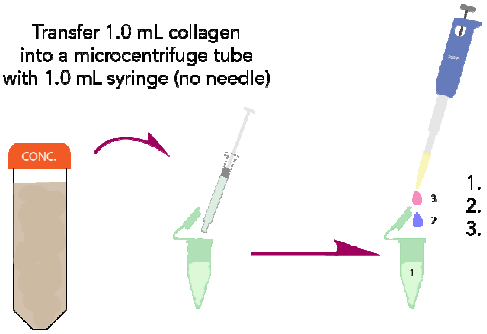

1. Collagen 1.0 mL
2. HEPES 10X buffer 125 µL, mix well
3. Cell (SMC or AHF) suspension 125 µL, mix well

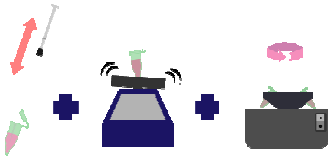

gental syringing | vortexing | microcentrifuge for 5~10 s
to rid bubbles

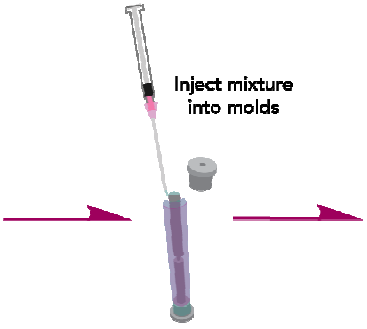

Inject mixture
into molds

Static Culture
in DMEM
at 37°C, 5% CO2
for 24 hr

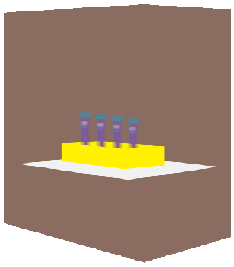

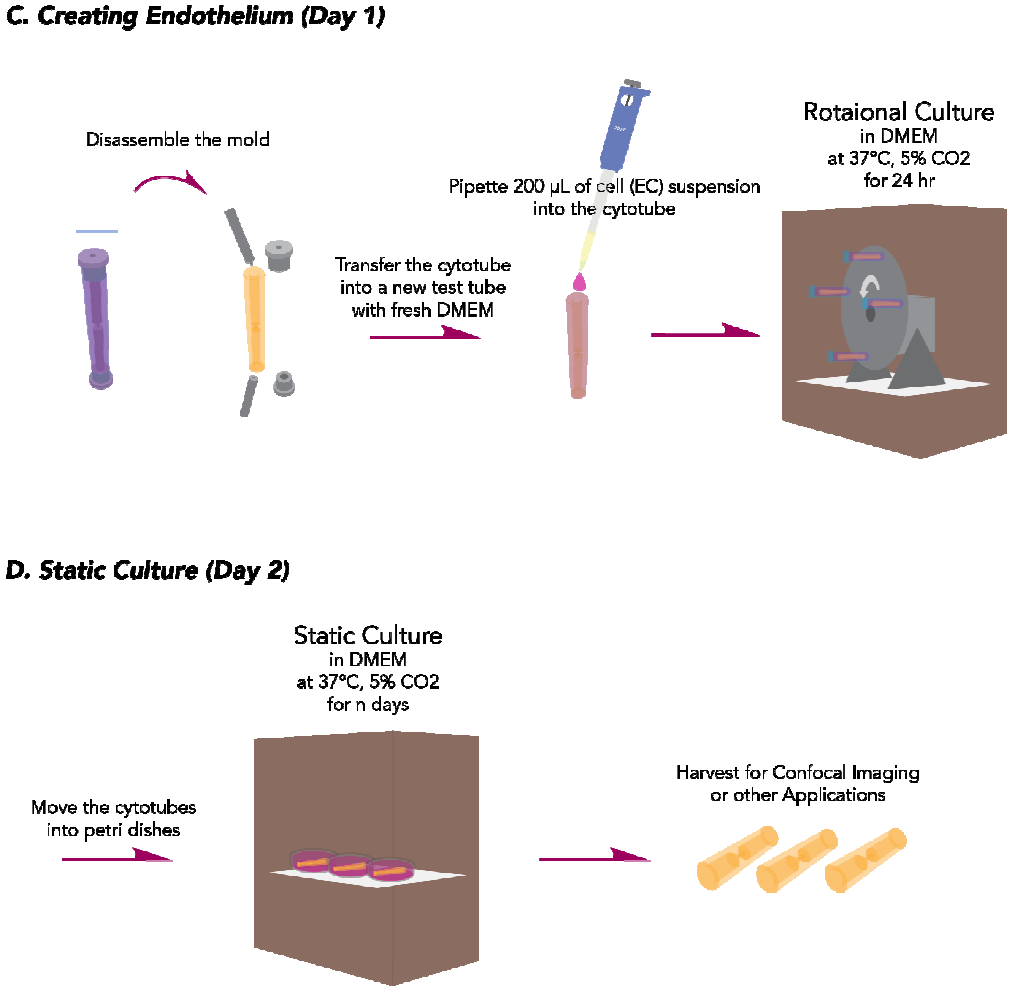

Figure 2.6 Step-by-step illustration of cytotube fabrication procedure.

CHAPTER 3
RESULTS AND DISCUSSION

3.1 CFD Modeling

In this analysis, input flows of mean velocity 0.5 cm/s, 1.0 cm/s and 2.0 cm/s were simulated to compare the effects of different inputs, and Reynolds number (Re), a dimensionless number that compares the fluid's inertia force with viscosity force, was applied to characterize the input flow type:

$$Re = \frac{2\rho R u_{mean}}{\mu}$$

where ρ is the fluid density, R is the inner radius of the channel, u_{mean} is the mean velocity of the input flow and μ is dynamic viscosity. When Reynolds number is higher than 4000 (inertia force significantly surpasses viscosity force), the flow is characterized as turbulent flow, whereas when Reynolds number is lower than 2100, the flow is regarded as laminar flow. [32] In this model, mean velocity of 0.5 cm/s, 1.0 cm/s and 2.0 cm/s gave rise to Reynolds numbers of 21.7, 43.4 and 86.7 respectively in the large channel (R=1.5 mm) and 100.0, 200.0, 400.1 in the constriction nozzle (R=0.325 mm), therefore were all considered laminar flow.

Figure 3.1 shows the results of CFD modeling in COMSOL Multiphysics®. The streamline and velocity field simulations indicated a region of recirculating flow posterior to the constriction nozzle and the size of this region depends on the mean flow velocity (Figure 3.2). This recirculating region dragged a portion of flow backwards, developing a divide where the velocity field dropped to zero, separating the flow into two

opposite directions. A proposed hypothesis is that the zero-velocity-field divide could have a high possibility to trap particles because of its stagnant flow condition, thus could be more susceptible to hyperlipidemia than forwarding flow regions. The wall shear rate isoline (gradient) simulation revealed a steep increase in shear rate in the narrowing nozzle and a dynamic shear rate fluctuation in the recirculating region. Shear rate can be related to the shear stress using the following equation:

$$\tau = \mu \frac{\partial u}{\partial y}$$

Where τ is shear stress, μ is dynamic viscosity, u is local fluid velocity and $\frac{\partial u}{\partial y}$ is local shear rate with respect to y-axis.

Numerous previous studies have investigated how shear stress could have affected EC and VSMC (vascular smooth muscle cell) phenotypic states. The majority of findings agreed that higher laminar shear stress inhibits VSMC proliferation and migration and increases VSMC apoptosis, whereas low or oscillatory shear stress induces VSMC phenotypic transformation to synthetic state and increases proliferation and migration through multiple regulatory pathways. Nonetheless, while low shear stress is considered to be more atherogenesis than high shear stress, both phenomena; however, have the potential to contribute to disease. [33] The three different types of shear stress – high, low and oscillating, will be generated simultaneously in different regions of the cytotube according to CFD modeling results; therefore, the model will be a useful tool to give us insights in the mechanical-force-induced cell behaviors in flow analysis.

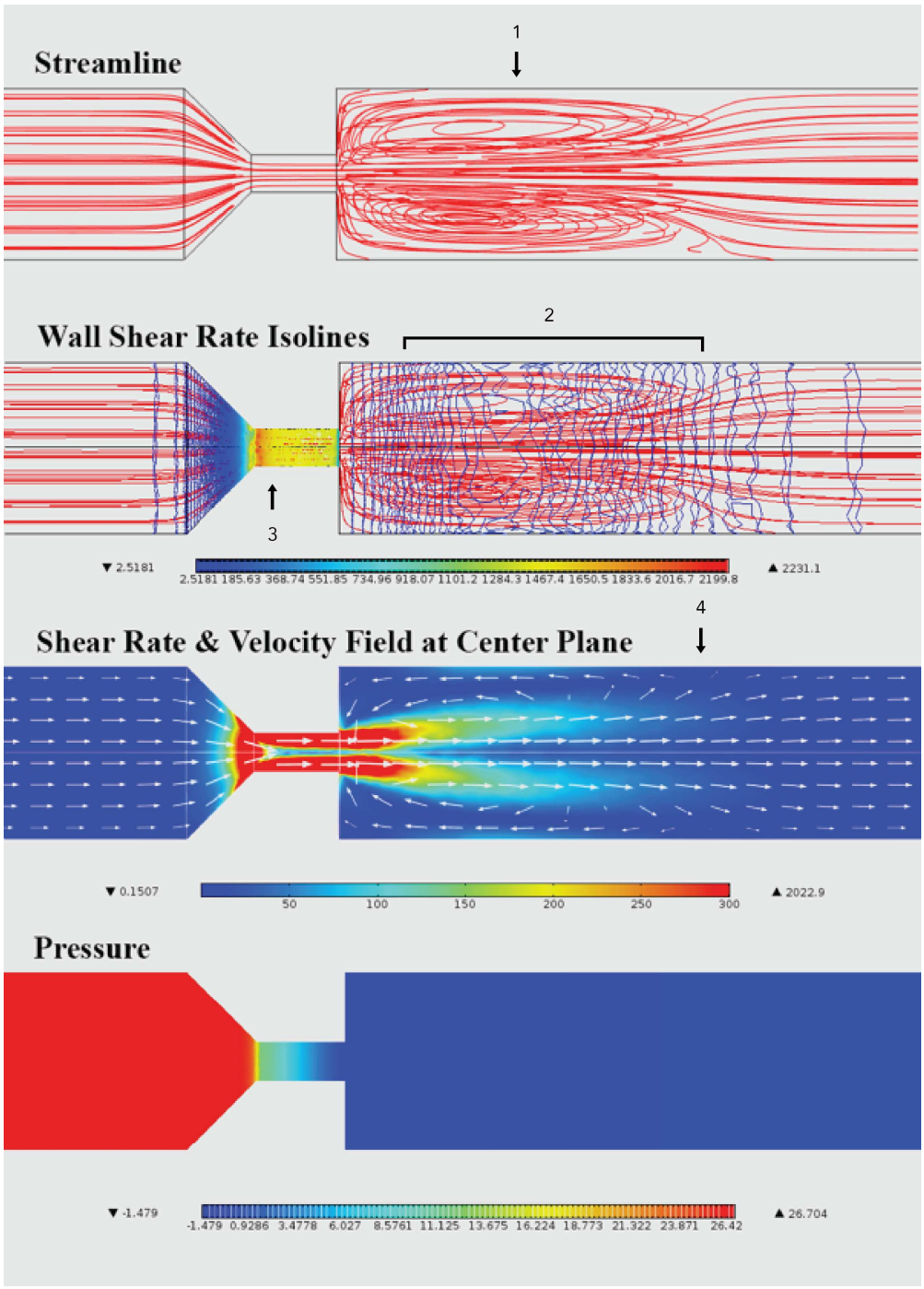

Figure 3.1 The streamline, wall shear rate, centerplane shear rate and velocity field as well as pressure gradient simulation with 0.5 cm/s mean velocity input. Indicated by the black arrows are (1) the recirculating region posterior to the nozzle, (2) the fluctuating graident of wall shear rate region, (3) the steep increse of shear rate region in the nozzel, and (4) the stagnant divide between backward and forward flow. These regions will help investigate shear-stress-induced cell behaviors in flow analysis.

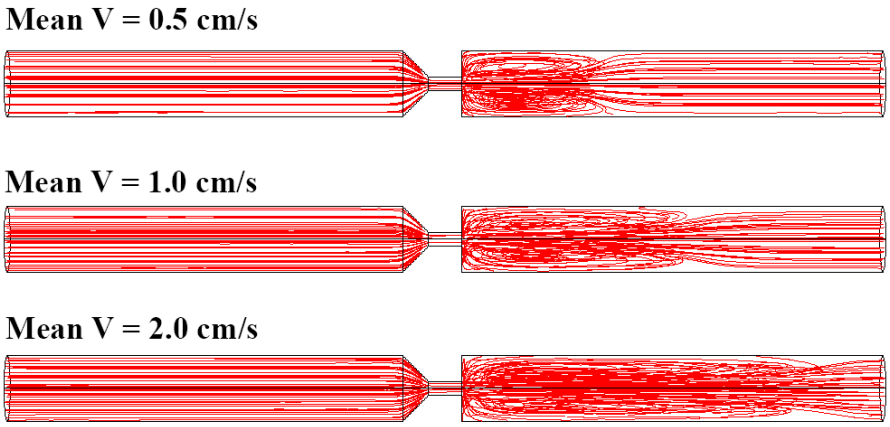

Figure 3.2 Mean velocity influences the size of the recirculating region. The higher the mean velocity, the larger the recirculating region. Despite being highly simplified, CFD modeling provides efficient prediction in where to look at.

3.2 Neutralizing Reagent for Acidic Collagen and the Look-Up Chart

The goal of these experiments was to determine the most suitable alkalinity of HEPES buffer that would bring the pH value of acidic collagen up to pH 7.4. Figure 3.3 shows that, for collagen of pH 5.27, 10X HEPES buffer of pH 7.84 should be used to neutralize the collagen. For collagen of pH 5.95, HEPES buffer of pH 7.70 would be the most appropriate choice. As for collagen of pH 6.64, the best buffer was pH 7.55 HEPES buffer. The linear relationship between acidity of collagen and alkalinity of neutralizing buffer enabled the establishment of a look-up chart for instant evaluation in future experiments, so only a small amount of collagen sample will need to be tested to ensure the correct final pH value. Figure 3.4 shows an example of how to find the neutralizing buffer for pH 6.30 collagen. First of all, find the approximate position of where pH 6.30 collagen would be when pH 7.7 HEPES buffer was added. This position can be found by

using interpolation method, where a line of slope ~ 0.9 that passes through the position. The slopes of the three data sets were found by using trend line function in Excel (Microsoft®) and the average was 0.89±0.07. The pH of neutralizing buffer should be found at the intersection where the predicted line passes through the pH 7.4 horizontal line, which is approximately pH 7.64 in this example.

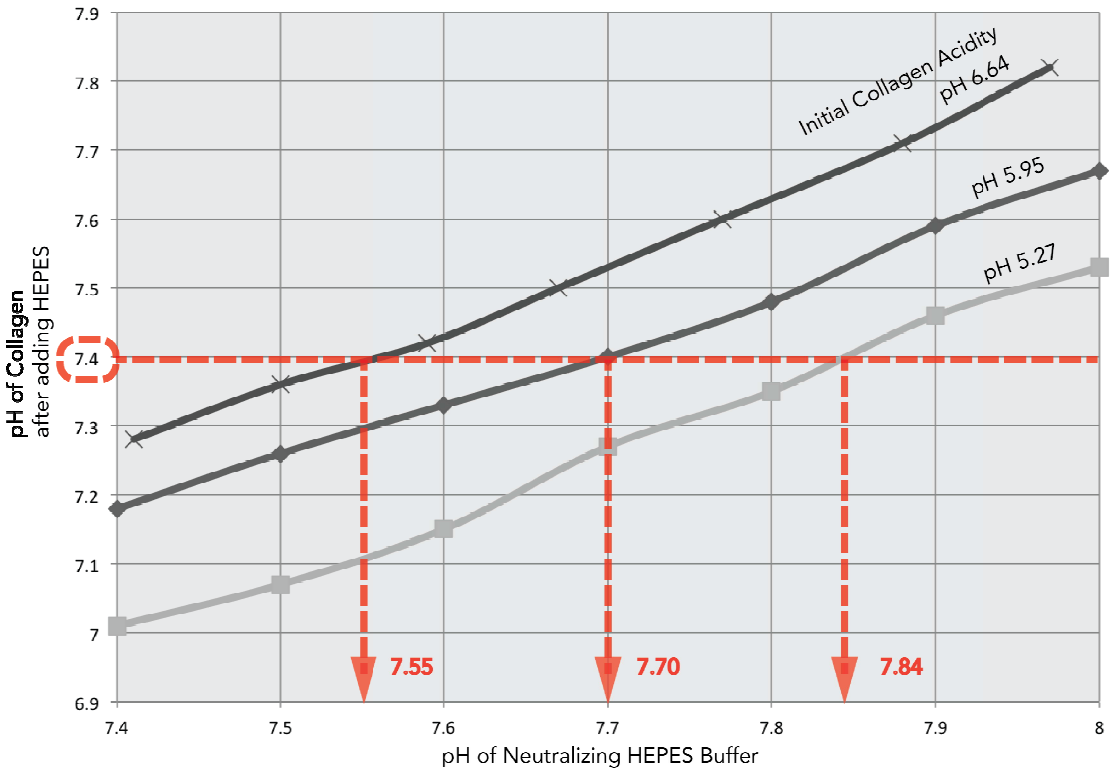

Figure 3.3 The corresponding neutralizing buffer for collagen of different acidity. Collagen of pH 6.64 requires pH7.55 HEPES buffer, whereas collagen of pH 5.95 requires pH 7.70 HEPES buffer and collagen of pH 5.27 requries pH 7.84 HEPES buffer.

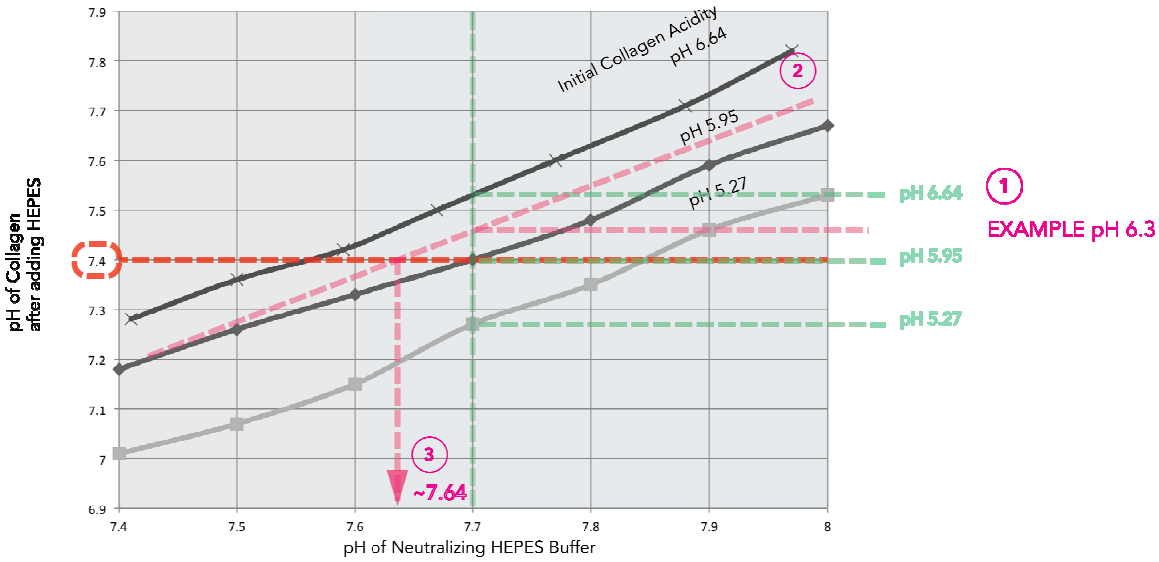

Figure 3.4 Example of utilizing the chart to predict pH value of the neutralizing buffer. First, find the position of the acidic collagen on the verticle pH 7.7 line. Second, predict a line with slope ~ 0.9 that passess through this position. Third, read the value on horizontal pH 7.4 line where the predicted line intersects. This pH value will be a close approximation to the most suitable neutrlazing buffer and will only require minimum tests to ensure the correct value.

3.3 Collagen Contractile Behavior of Cells in the Cytotube

Three groups of cytotubes – SMC-only, SMC+EC and EC-only, each contained 4 tubes, were fabricated at the same time and cultured for 10 days starting from collagen polymerization. Figure 3.5A shows the change in length of each group of cytotubes versus time. The contractile behavior of cells was most pronounced in cytotubes seeded with SMCs, which caused the cytotubes to shrink both lengthwise and widthwise. EC-only cytotubes had almost no shrinkage (4±1%) within the same time frame as the other two groups, whereas both SMC-only and SMC+EC co-cultured cytotubes showed noticeable reduction in dimensions. Interestingly, while SMC-only cytotubes became 56±5% shorter after 10 days of static culturing, the SMC+EC co-cultured cytotubes had

only decreased 29±5% in length. This observation may be in agreement of previous studies on EC/SMC co-culturing systems, which found that when ECs are exposed to normal level of shear stress, the reduction of matrix metalloprotease (MMP), platelet-derived growth factor (PDGF), transforming growth factor (TGF) all inhibit SMC proliferation, migration and protein secretion. However, when ECs are exposed to low shear stress or no shear stress, the upregulation of theses factors may lead to the opposite results and induce the SMC to transform into synthetic phenotype, which is considered to be one of the risk factors of atherogenesis. [33]

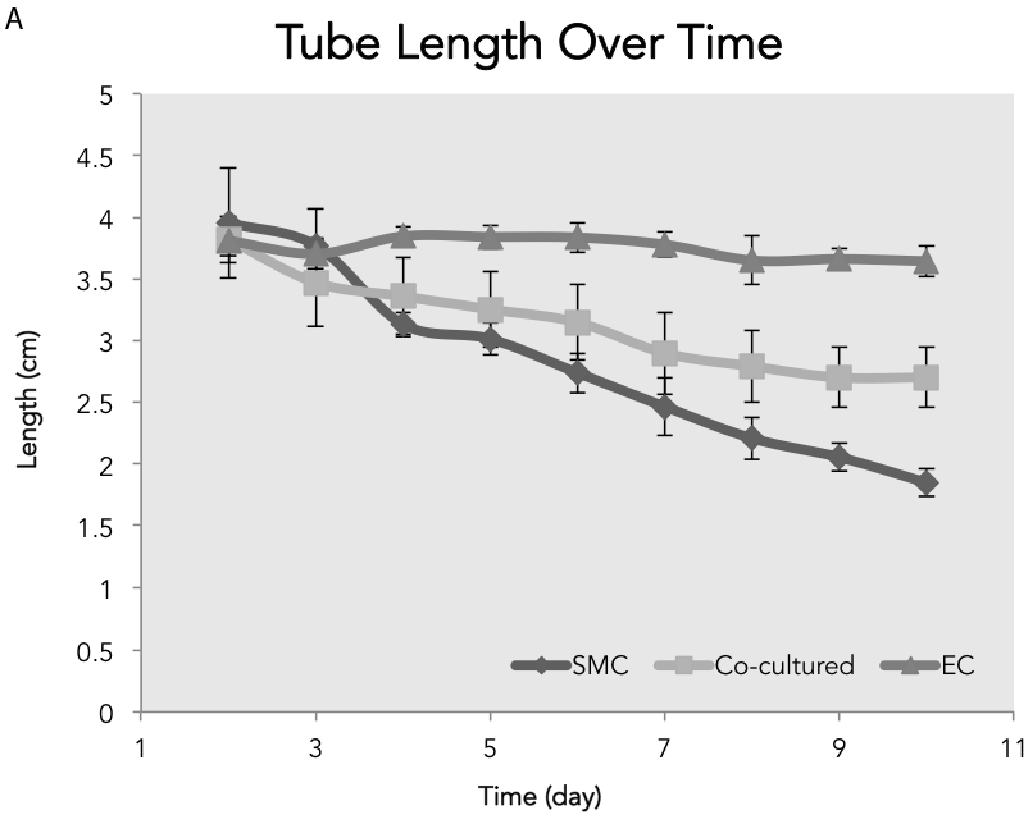

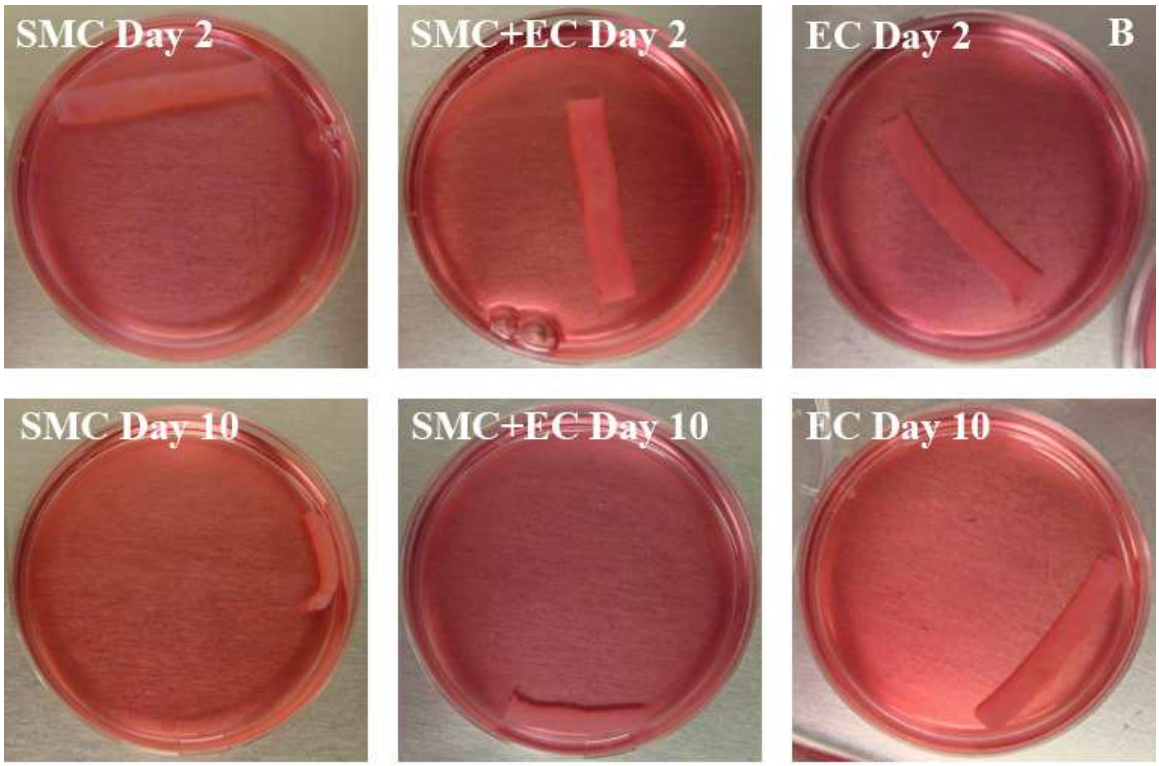

Figure 3.5 (A)Tube length shrinkage over time in static culture due to myocyte contractility. SMC-only cytotubes shows the highest level of shrinkage (56±5%), followed by EC+SMC cytotubes (29±5%). EC-only cytotubes shows almost no shrinkage in 10 days of static culture. (4±1%) The SMC-only cytotubes had a linear shrinking trend until day 10, while SMC+EC ones had a tendency to stop shrinking between day 9 and day 10. (B) The appearance of the same cytotubes seeded with different cell types on day 2 and day 10. Dimension was acquired by measuring cytotubes in the images with ImageJ. The reference length is the diameter of the 60 mm petri dish.

3.4 Confocal Imaging

3.4.1 Optimization with Adult Rat Heart Fibroblast (AHF)

Rat heart fibroblasts were first used to examine the validity of the "creating muscular wall" procedure, in which solubilized collagen was mixed with cells while polymerizing into tubular shape. Figure 3.6 is the result of AHFs seeded within the collagen scaffold over time. The first panel (A~E) shows the morphology of AHFs within collagen from day 1 to day 5. On day 1 (A), after 24 hours of static culture within

collagen, cells were mostly still in rounded up, retracted shape. However, on day 2 and afterwards (B-E), AHFs began elongating and spreading, displaying dendritic, stellate morphology, which is typical on in vivo mesenchymal cells. Together these cells also had mesenchyme-like distribution across the scaffold that is usually characterized as a natural "resting state" of fibroblasts found in expanses of extracellular matrix in vivo connective tissues.

The second panel (F~H) shows the morphology of AHFs found on the luminal surface from day 4 to day 6. Here a markedly different morphology from that of cells within collagen was observed in f-actin stress fibers (green) and SMαA (red). Not only the cells displayed a flattened or squamous morphology that is usually not characterized in mesenchymal cells, but the sheet-like spreading of stress fibers within the cells (G, right arrow) and organized SMαA filaments (G, left arrow) also implied a phenotypic change from quiescent cells to activated cells. [34]–[36] Activated fibroblasts result in a variety cellular activity including migration, proliferation, ECM production and differentiation. While detailed cell molecular analysis may be required to explore the phenotypic state of the AHFs in the current model, the confocal micrographs have shown that the proposed fabrication method was able to support cell survival within the collagen scaffold with or without phenotypic transformation. The third panel (I~K) is the cross-sectional view of the barrier-like, or endothelium-like, wall formation on the surface of the collagen scaffold. Increasing confluency over time can be observed by comparing the fenestrated layer in Day 4 with the sealed layer in Day 5 and Day 6. Here, the cell adapted a cobblestone-like phenotype with characteristic cortical actin filaments.

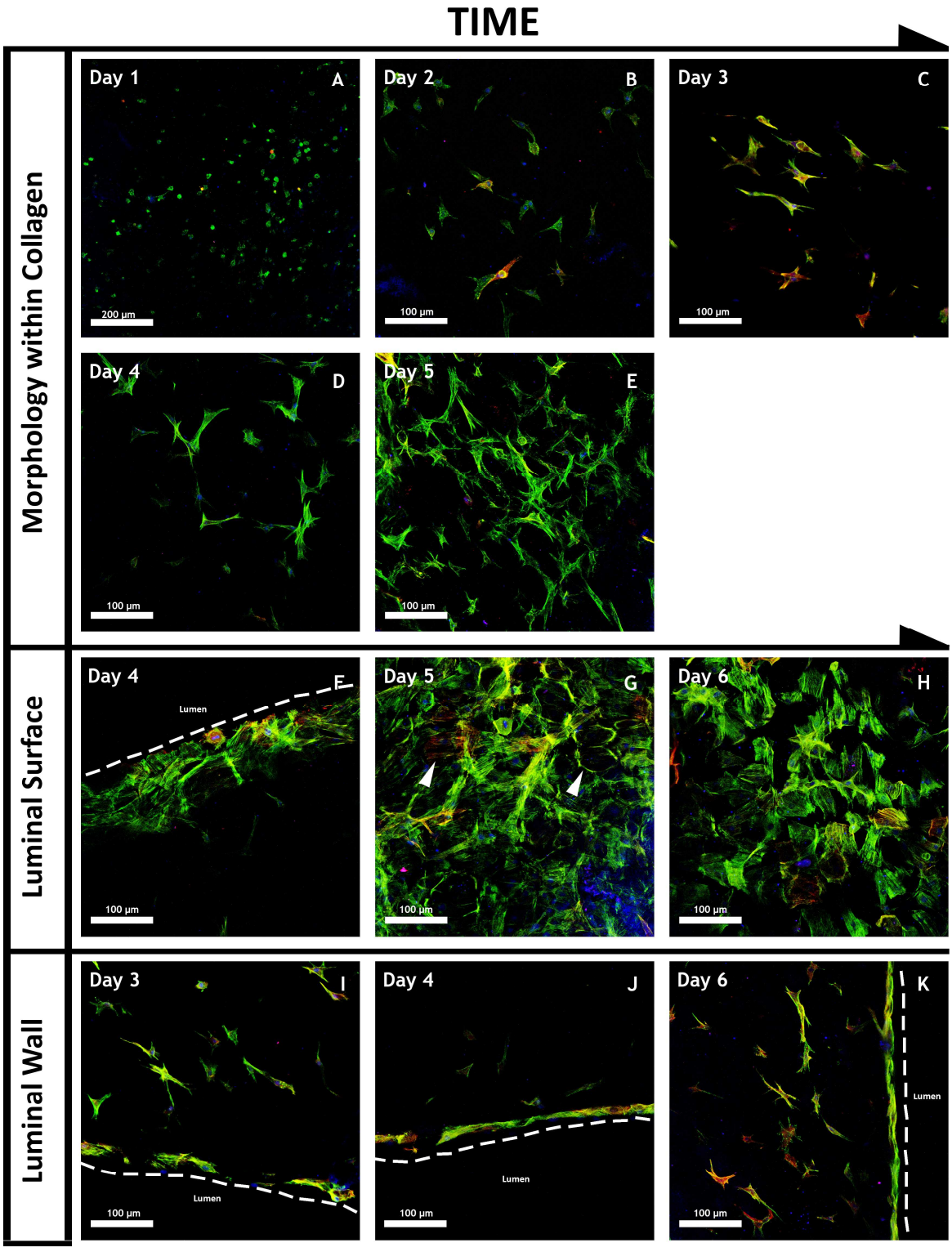

Figure 3.6 Morphology of adult rat heart fibroblasts (AHF) cultured within collagen scaffold at various sties over time. All samples shown were stained with phalloidin (green), DAPI (blue) and Cy3-SMαA (red).

3.4.2 EC-only Cytotubes

Figure 3.7 shows the results of creating endothelium with ECs. The 24-hour specimens were harvested immediately after the rotational culture, whereas the rest of the specimens were all collected in static culture at the time points indicated. After 24 hours of rotational culture, sporadic cell clusters were found on the luminal side of the cytotube (A, E). At this early time point, although cell population was not dense and cellular shape was rather globular, cell spreading could already be seen (A). 48-hour specimens also showed globular cells clusters (B, F), but the cortical actin filaments surrounding the cytoplasm between adjacent cells imply the formation of ECs' cell-to-cell junctions, which is an important characteristic of ECs to carry out phenotypic barrier functions. [37] The squamous, confluent endothelium was observed on the luminal surface of the cytotubes after 5~7 days of static culture. (C, G, D, H)

3.4.3 SMC-only Cytotubes

Morphology of SMCs within the collagen scaffold was imaged transversely across the constriction nozzle regions. Individual Images of 450 μm×450 μm area were tiled into long strips in Photoshop (Adobe®). Figure 3.8 shows half of the strips of day 1, day 3, day 5 and day 7. On day 1, immediately after the cytotubes are removed from the mold, SMCs within collagen were in a rounded-up morphology typical for trypsinized cells throughout the scaffold. Only a small number of cells close to the outer wall, where the cells were in direct contact of the dialysis membrane, showed elongated, spindle-shaped stretching along longitudinal direction of the cytotube. On day 3, day 5 and day 7, SMCs displayed a morphological transition spatially from spindle-shaped or spherical

shaped cells in the luminal side, stellate cells near the outer wall, to a confluent layer of SMCs aligning along longitudinal direction of the cytotube.

3.4.3.1 Relative Spatial Distribution Analysis – F-actin of SMCs

Because a stellate-shaped cell takes up a larger area than a spindle-shaped or rounded-up cell, phalloidin-stained f-actin signal (green) was chosen to help analyze the relative spatial distribution of SMC morphology with ImageJ's built-in function "Gel Analysis". This tool gives a function of total widthwise intensity of pixels versus lengthwise position. The entire strip's intensity-to-position map was then equally divided into 10 portions along x-axis, in which the detected signals were summed up such that these areas could be compared to that of the total signal. Although this analysis require further optimizations in regards nuclei distribution so that it can be normalized to the higher amount of signals caused by denser cell population in some areas (such as the higher density of cells close to lumen in Figure 3.8 D1). This analysis does reveal an approximation of relative spatial variations in cell spreading, proliferation and migration across the scaffold over time. Figure 3.9B shows the result of relative f-actin spatial distribution versus relative position on day 1, day 3, day 5 and day 7. An increasing trend of relative amount of f-actin on the outer wall over time and decreasing trend in the luminal region can be seen in the chart. Combined with the qualitative micrograph data, we hypothesized that SMCs on the outer wall were exhibiting synthetic phenotype, characterized by having higher proliferation, migration and ECM synthesis rate and may be induced by the serum containing culture media. [38] In contrast, the SMCs embedded deeper in the scaffold could have been in contractile state, contributing to the gross

shrinkage behavior of the cytotubes. This hypothesis requires to be investigated with a more detailed cell molecular analysis and controlled presets in confocal microscopy.

3.4.5 RAEC+RASMC Co-culture Cytotubes

When ECs and SMCs were co-cultured on the cytotube, an endothelium-like "tissue" was found along the luminal wall (A) along with mesenchymal-like cells (B) within the construct wall after 6 days. The detection of both vWF (green), an endothelial cell specific marker, and SMαA (red) in the same cells implied that these cells were endothelial cells undergoing endothelial-to-mesenchymal transformation (EnMT) and were migrating into collagen scaffold, where synthetic SMCs might secrete high levels of PDGF-BB that induced the transformation. [39] Although the multilayered fabrication technique have resulted in vivo-like morphology in both intimal and medial walls, lacking a control group of single cell type sample with the same immunofluorescent stainings made the true identity of the cells unclear. Artifacts generated during staining and confocal microscopy were all able to deviate the generic signals.

Taking these considerations into account, ongoing efforts will include: (1) A systemic comparison between cytotubes seeded with single cell type (EC- or SMC-only) and multiple cell types (EC+SMC). To do so, the same combination of immunofluorescent stainings, that is, anti-vWF or anti-VE-cadherin, anti-SMαA and DAPI, will need to be applied to all different samples (EC-only, SMC-only, and EC+SMC cytotubes) to determine whether the physiological phenotypes of cells are altered due to cell-ECM or cell-cell interactions. (2) RNA expression analysis on EC, SMC and EC+SMC cytotubes with real-time reverse transcriptase PCR (qRT-PCR).

Some important markers can help determine the phenotype of cells of interests. Rose & Babensee, 2007 [40] uncovered phenotypic change in a human aortic smooth muscle cells (HASMC)/human aortic endothelial cells (HAEC) co-culturing system. In the study, contractile HASMCs, less secretory HASMCs and more secretory HASMCs co-cultured with quiescent HAECs were compared. They found that the contractile HASMCs had organized SMαA filaments, low levels of interlukin-8 (IL-8) and monocyte chemotactic protein-1 (MCP-1) secretion, and low expression of intracellular adhesion molecule-1 (ICAM-1) and vascular cell adhesion molecule-1 (VCAM-1). However, more secretory HASMCs showed diffuse, unorganized SMαA and increased levels in all the markers mentioned above. Less secretory HASMCs had more contractile-like characteristics in 48 hours of co-culturing, but became more secretory-like later. Other markers for EC's such as platelet endothelial cell adhesion molecule-1 (PECAM-1)[41] and procoagulant factor von Willebrand factor (vWF) [42] and SMC's such as platelet-derived growth factor (PDGF) [43], collagen type I (Col I), collagen type III (Col III), and matrix metalloproteinases (MMP) [44], [45] are all associated with atherogenesis and should be investigated as well. These studies will help evaluate the cellular behaviors in the 3D co-culturing system, and facilitate the development of a more in vivo like cytotube that can be applied in a variety of in vitro studies.

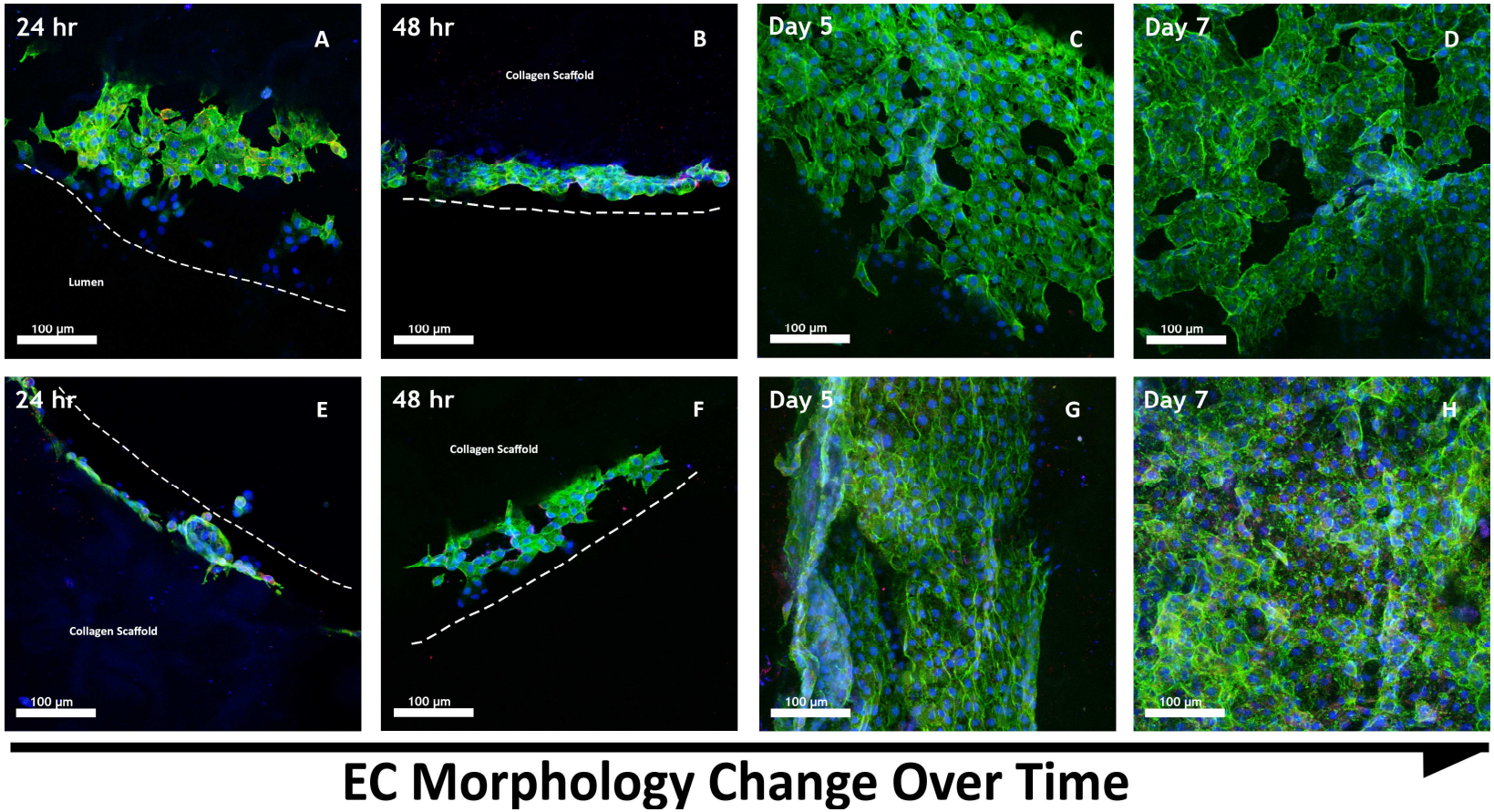

Figure 3.7 Morphology of ECs seeded in the luminal surface of the EC-only cytotube over time. All samples shown were stained with phalloidin (green), DAPI (blue) and Cy3-SMαA (red).

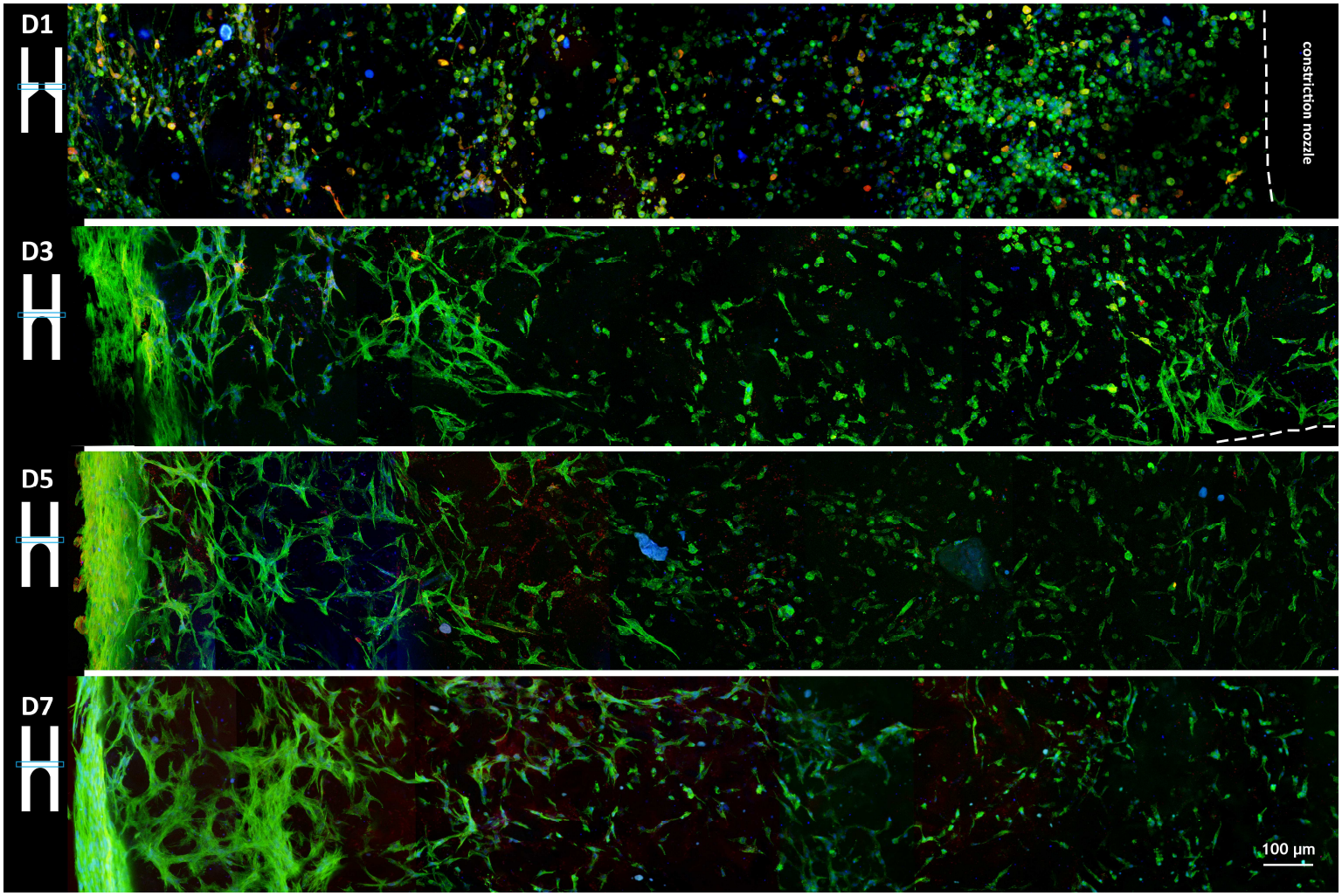

Figure 3.8 SMC morphology within the cytotubes from day 1 to day 7 in static culture. The legend shown on top-right indicates the location of the images in the sections All samples shown were stained with phalloidin (green), DAPI (blue) and Cy3-SMαA (red).

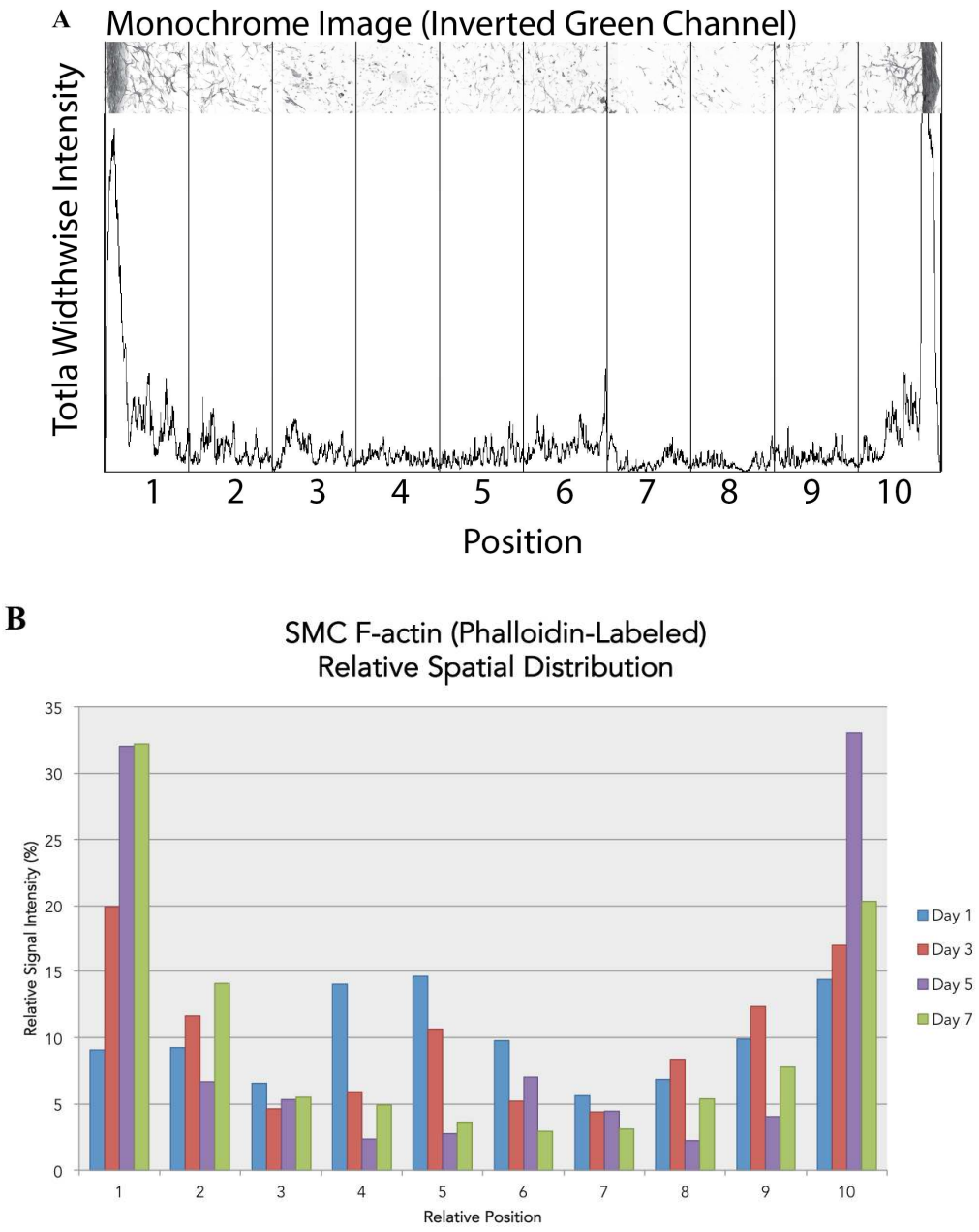

Figure 3.9 Relative spatial distribution of f-actin over time. The upper graph (A) demonstrates the intensity-to-position data collected from a tiled strip using the ImageJ "Gel Analysis" function. The graph was equally divided into 10 portions on x-axis and the area in each portion was represented in percentile in the new graph. (B) An increasing trend of relative amount of signal over time on the outer wall (position 1, 2, 3, 8, 9, 10) and decreasing trend in the luminal region (position 4 ~ 7) can be observed over time.

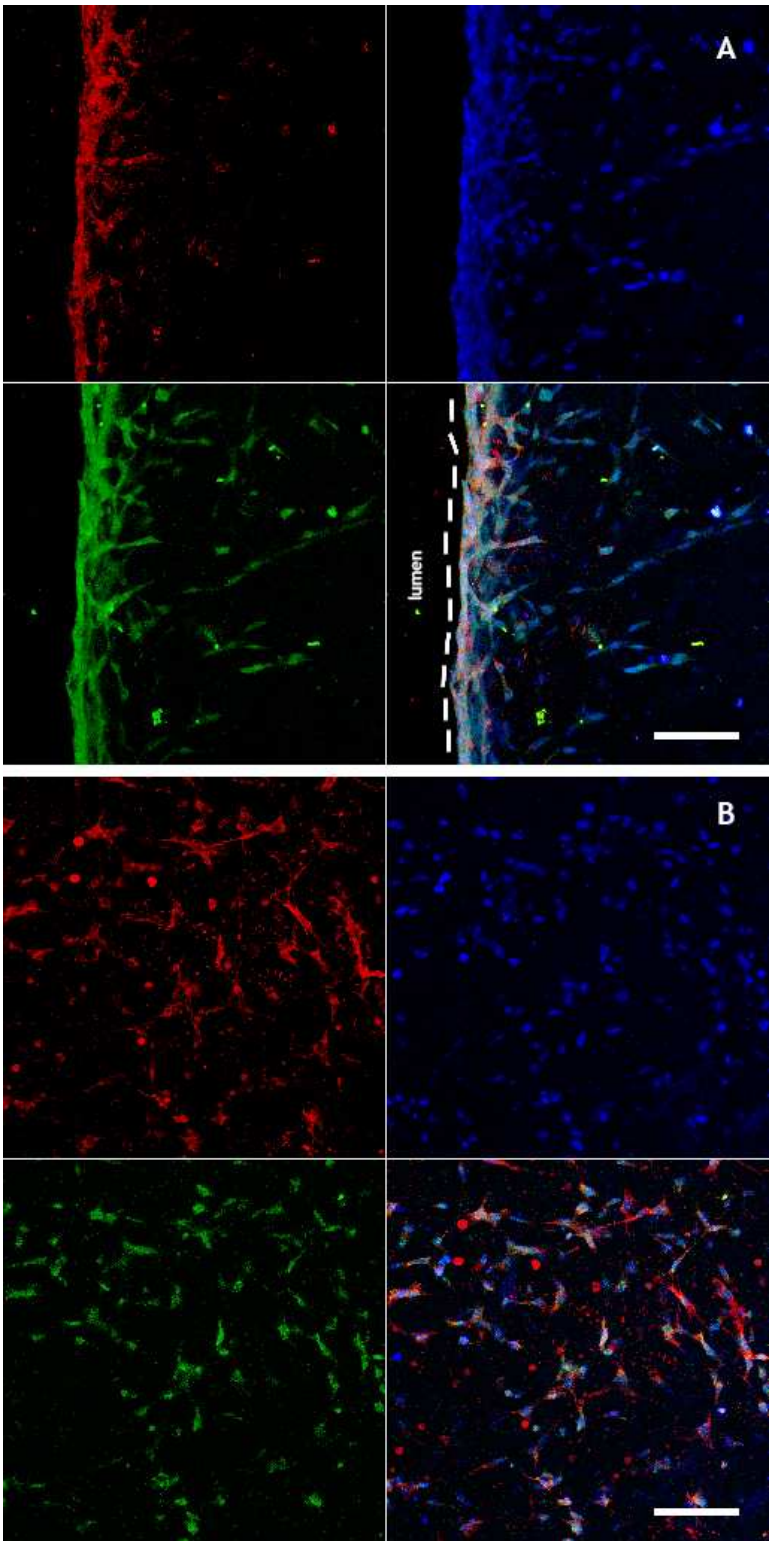

Figure 3.10 Endothelium-like structure on the luminal wall (A) and mesenchymal-like cells within the scaffold (B). All samples shown were stained with FITC-vWF (green), DAPI (blue) and Cy3-SMαA (red). Scale bar : 100 µm.

CHAPTER 4
CONCLUSION & FUTURE DIRECTIONS

4.1 Conclusion

This study generated a novel fabrication method for a three-dimensional in vitro cell-culturing model with specialized luminal geometry, which has the potential to support in vivo-like morphologies of vascular cells (AHF, EC and SMC), generate unique flow patterns, and therefore serve as a model of atherogenesis. By fine-tuning the pH value of solubilized collagen gel with concentrated HEPES buffer prior to cell seeding, a suitable environment was created for cells to be co-polymerized with collagen. Additionally, the large MWCO of the dialysis tubing used as the sheath for the mold allows for rapid small molecule exchange, which enabled quick osmotic balancing and nutrients and metabolic wastes transportation, while allowing for the cell/collagen mixture to polymerize into desired shape. Both factors optimized the environment for cells cultured within solubilized collagen. Confocal microscopy studies found that cells grown within and on the cytotube developed in vivo cell morphologies and cellular arrangements typical if vascular tissues in 7~10 days of static culture. This proposed model has the potential to be applied to a variety of multicellular 3D models of pathogenesis, and could also influence vascular tissue engineering studies.

4.2 Future Directions

Future studies need to focus on the effect of flow on the cellular response of different cell types in cytotubes. It has been reported that when being subjected to flow or mechanical stresses in vitro, endothelial cells and smooth muscle cells exhibited an oriented morphology aligning to the external force, which resembles the in vivo appearance of both cell types. [46], [47] This phenomenon is expected to be seen in the resulting cytotubes when they undergo flow culture. Flow culture not only will introduce shear stress on the inner wall of the cytotube, but the tensile stress caused by suturing the cytotube onto the bioreactor, as well as the circumferential pressure exerted on the wall by the luminal fluid will also provide a source of mechanical force that could influence the morphology of seeded cells. By manipulating these factors in an introductory flow culture, a more in vivo-like 3D model can hopefully be achieved. Also, because of myocyte contractility that resulted in shrinkage in diameter of the cytotubes, it is proposed that if the metal molds be reinserted into the cytotube in an early stage or be left in the cytotube for prolonged time, the circumferential stress produced by expanding the diameter or by resisting shrinkage may be another viable method to induce circularly aligned smooth muscle cells.

Besides further examinations and applications of the cytotubes, some variations and improvements will be considered to increase current model's versatility. In fact, the geometry of the current model was designed partially according to the materials adopted in this project, that is, the dialysis tubing. Although dialysis tubing has been an exceptional container to simultaneously allow for cell survival and collagen polymerization, the resulting shape of a model using such material is limited. In fact,

seeing that bifurcating sites in arteries are found to have higher risks of atherogenesis, fabricating a branching model may be more *in vivo*-mimicking and applicable. Recently, 3D bio-printing technology has drastically increased the possibility in reifying conceptual tissue-engineering designs. With the choices of materials being increasingly flexible, 3D bioprinting can potentially be a stairway to a more complex in vitro model. [48], [49]

REFERENCES

[1] R. C. Thompson, A. H. Allam, G. P. Lombardi, L. S. Wann, M. L. Sutherland, J. D. Sutherland, M. A.-T. Soliman, B. Frohlich, D. T. Mininberg, J. M. Monge, C. M. Vallodolid, S. L. Cox, G. Abd el-Maksoud, I. Badr, M. I. Miyamoto, A. el-Halim Nur el-din, J. Narula, C. E. Finch, and G. S. Thomas, "Atherosclerosis across 4000 years of human history: the Horus study of four ancient populations," *Lancet*, vol. 381, no. 9873, pp. 1211–1222, Apr. 2013.

[2] M. Madjid, I. Aboshady, S. W. Casscells, R. Virmani, and J. T. Willerson, "History of Atherosclerosis and Vulnerable Plaque Research," in *The Vulnerable Atherosclerotic Plaque*, Blackwell Publishing, 2006, pp. 1–17.

[3] A. S. Go, D. Mozaffarian, V. L. Roger, E. J. Benjamin, J. D. Berry, M. J. Blaha, S. Dai, E. S. Ford, C. S. Fox, S. Franco, H. J. Fullerton, C. Gillespie, S. M. Hailpern, J. a Heit, V. J. Howard, M. D. Huffman, S. E. Judd, B. M. Kissela, S. J. Kittner, D. T. Lackland, J. H. Lichtman, L. D. Lisabeth, R. H. Mackey, D. J. Magid, G. M. Marcus, A. Marelli, D. B. Matchar, D. K. McGuire, E. R. Mohler, C. S. Moy, M. E. Mussolino, R. W. Neumar, G. Nichol, D. K. Pandey, N. P. Paynter, M. J. Reeves, P. D. Sorlie, J. Stein, A. Towfighi, T. N. Turan, S. S. Virani, N. D. Wong, D. Woo, and M. B. Turner, *Heart disease and stroke statistics--2014 update: a report from the American Heart Association.*, vol. 129, no. 3. 2014, pp. e28–e292.

[4] C. D. Mathers and D. Loncar, "Projections of global mortality and burden of disease from 2002 to 2030.," *PLoS Med.*, vol. 3, no. 11, p. e442, Nov. 2006.

[5] S. Mendis, P. Puska, and B. Norrving, *Global atlas on cardiovascular disease prevention and control.* 2011.

[6] D. S. Jones, S. H. Podolsky, and J. a Greene, "The burden of disease and the changing task of medicine.," *N. Engl. J. Med.*, vol. 366, no. 25, pp. 2333–8, Jun. 2012.

[7] P. Cullen, J. Rauterberg, and S. Lorkowski, "The pathogenesis of atherosclerosis.," *Handb. Exp. Pharmacol.*, vol. 1, no. 170, pp. 3–70, Jan. 2005.

[8] F. Epstein and R. Ross, "Atherosclerosis - An Inflammatory Disease," *N. Engl. J. Med.*, pp. 115–126, 1999.

[9] Y. Hoi, Y.-Q. Zhou, X. Zhang, R. M. Henkelman, and D. a Steinman, "Correlation between local hemodynamics and lesion distribution in a novel aortic regurgitation

murine model of atherosclerosis.," *Ann. Biomed. Eng.*, vol. 39, no. 5, pp. 1414–22, May 2011.

[10] C. G. Caro, "Discovery of the role of wall shear in atherosclerosis.," *Arterioscler. Thromb. Vasc. Biol.*, vol. 29, no. 2, pp. 158–61, Feb. 2009.

[11] H. F. Younis, M. R. Kaazempur-Mofrad, R. C. Chan, a G. Isasi, D. P. Hinton, a H. Chau, L. a Kim, and R. D. Kamm, "Hemodynamics and wall mechanics in human carotid bifurcation and its consequences for atherogenesis: investigation of inter-individual variation.," *Biomech. Model. Mechanobiol.*, vol. 3, no. 1, pp. 17–32, Sep. 2004.

[12] F. B. Gessner, "Brief Reviews: Hemodynamic Theories of Atherogenesis," *Circ. Res.*, vol. 33, no. 3, pp. 259–266, Sep. 1973.

[13] J. Ravensbergen, J. W. Ravensbergen, J. K. B. Krijger, B. Hillen, and H. W. Hoogstraten, "Localizing Role of Hemodynamics in Atherosclerosis in Several Human Vertebrobasilar Junction Geometries," *Arterioscler. Thromb. Vasc. Biol.*, vol. 18, no. 5, pp. 708–716, May 1998.

[14] P. a VanderLaan, C. a Reardon, and G. S. Getz, "Site specificity of atherosclerosis: site-selective responses to atherosclerotic modulators.," *Arterioscler. Thromb. Vasc. Biol.*, vol. 24, no. 1, pp. 12–22, Jan. 2004.

[15] R. Timpl, H. Rohde, and P. Robey, "Laminin--a glycoprotein from basement membranes," *J. Biol. …*, 1979.

[16] D. A. Simon Davis and C. R. Parish, "Heparan sulfate: a ubiquitous glycosaminoglycan with multiple roles in immunity.," *Front. Immunol.*, vol. 4, no. December, p. 470, Jan. 2013.

[17] A. Patel, B. Fine, M. Sandig, and K. Mequanint, "Elastin biosynthesis: The missing link in tissue-engineered blood vessels.," *Cardiovasc. Res.*, vol. 71, no. 1, pp. 40–9, Jul. 2006.

[18] M. R. Roach and S. H. Song, "Variations in strength of the porcine aorta as a function of location," *Clin. Invest. Med.*, vol. 17, no. 4, p. 308—318, Aug. 1994.

[19] T. C. Gasser, R. W. Ogden, and G. a Holzapfel, "Hyperelastic modelling of arterial layers with distributed collagen fibre orientations.," *J. R. Soc. Interface*, vol. 3, no. 6, pp. 15–35, Feb. 2006.

[20] A. Rudijanto, "The role of vascular smooth muscle cells on the pathogenesis of atherosclerosis.," *Acta Med. Indones.*, vol. 39, no. 2, pp. 86–93.

[21] C. L. VanPutte, J. Regan, A. Russo, R. R. Seeley, T. D. Stephens, and P. Tate, "Structural features of blood vessels," in *Seeley's anatomy & physiology*, 10th ed., New York, NY : McGraw-Hill, ©2014, 2014, pp. 710–716.

[22] H. Chen, Y. Liu, M. N. Slipchenko, X. Zhao, J.-X. Cheng, and G. S. Kassab, "The layered structure of coronary adventitia under mechanical load.," *Biophys. J.*, vol. 101, no. 11, pp. 2555–62, Dec. 2011.

[23] M. W. Majesky, X. R. Dong, V. Hoglund, W. M. Mahoney, and G. Daum, "The adventitia: a dynamic interface containing resident progenitor cells.," *Arterioscler. Thromb. Vasc. Biol.*, vol. 31, no. 7, pp. 1530–9, Jul. 2011.

[24] B. C. Tieu, X. Ju, C. Lee, H. Sun, W. Lejeune, A. Recinos, A. R. Brasier, and R. G. Tilton, "Aortic adventitial fibroblasts participate in angiotensin-induced vascular wall inflammation and remodeling.," *J. Vasc. Res.*, vol. 48, no. 3, pp. 261–72, Jan. 2011.

[25] C. Weinberg and E. Bell, "A blood vessel model constructed from collagen and cultured vascular cells," *Science (80-.).*, vol. 231, no. May 2014, pp. 397–400, 1986.

[26] S. C. Schutte and R. M. Nerem, "Blood Vessel Tissue Engineering," in *Applications of Biomaterials in Functional Tissue Engineering*, 2005, pp. 1237–1246.

[27] T. F. Linsenmayer, "Collagen," in *Cell Biology of Extracellular Matrix*, 2nd ed., E. D. Hay, Ed. Plenum Publishing Corporation, 1991, pp. 7–44.

[28] P. Singh, S. Benjakul, S. Maqsood, and H. Kishimura, "Isolation and characterisation of collagen extracted from the skin of striped catfish (Pangasianodon hypophthalmus)," *Food Chem.*, vol. 124, no. 1, pp. 97–105, Jan. 2011.

[29] K. Hanai, T. Kojima, M. Ota, J. Onodera, and N. Sawada, "Effects of atelocollagen formulation containing oligonucleotide on endothelial permeability.," *J. Drug Deliv.*, vol. 2012, p. 245835, Jan. 2012.

[30] J. Kestin, M. Sokolov, and W. A. Wakeham, "Viscosity of Liquid Water in the Range -8°C to 150°C," *J. Phys. Chem. Ref. Data*, vol. 7, no. 3, pp. 941–948, 1978.

[31] M. J. Yost, C. F. Baicu, C. E. Stonerock, R. L. Goodwin, R. L. Price, J. M. Davis, H. Evans, P. D. Watson, C. M. Gore, J. Sweet, L. Creech, M. R. Zile, and L. Terracio, "A novel tubular scaffold for cardiovascular tissue engineering.," *Tissue Eng.*, vol. 10, no. 1–2, pp. 273–84, 2004.

[32] F. A. Morrison, “Quick Star: The mechanical energy balance,” in *An Introduction to Fluid Mechanics*, New York, NY: Cambridge University Press, 2013, pp. 8–49.

[33] J. Qiu, Y. Zheng, J. Hu, D. Liao, H. Gregersen, X. Deng, Y. Fan, and G. Wang, “Biomechanical regulation of vascular smooth muscle cell functions: from in vitro to in vivo understanding.,” *J. R. Soc. Interface*, vol. 11, no. 90, p. 20130852, Jan. 2014.

[34] F. Grinnell, “Fibroblast biology in three-dimensional collagen matrices,” *Trends Cell Biol.*, vol. 13, no. 5, pp. 264–269, May 2003.

[35] F. Grinnell, C. Ho, E. Tamariz, D. J. Lee, and G. Skuta, “Dendritic Fibroblasts in Three-dimensional Collagen Matrices,” vol. 14, no. February, pp. 384–395, 2003.

[36] H. M. Langevin, N. A. Bouffard, G. J. Badger, J. C. Iatridis, A. K. Howe, and M. Helene, “Dynamic fibroblast cytoskeletal response to subcutaneous tissue stretch ex vivo and in vivo,” vol. 05405, pp. 747–756, 2005.

[37] E. Dejana, M. Corada, and M. Lampugnani, “Endothelial cell-to-cell junctions,” *FASEB J.*, vol. 9, no. July, 1995.

[38] E. M. Rzucidlo, K. a Martin, and R. J. Powell, “Regulation of vascular smooth muscle cell differentiation.,” *J. Vasc. Surg.*, vol. 45 Suppl A, pp. A25–32, Jul. 2007.

[39] G. Krenning, J. R. a J. Moonen, M. J. a van Luyn, and M. C. Harmsen, “Vascular smooth muscle cells for use in vascular tissue engineering obtained by endothelial-to-mesenchymal transdifferentiation (EnMT) on collagen matrices,” *Biomaterials*, vol. 29, no. 27, pp. 3703–3711, Sep. 2008.

[40] S. L. Rose and J. E. Babensee, “Complimentary endothelial cell/smooth muscle cell co-culture systems with alternate smooth muscle cell phenotypes.,” *Ann. Biomed. Eng.*, vol. 35, no. 8, pp. 1382–90, Aug. 2007.

[41] E. Cenni, D. Granchi, C. R. Arciola, G. Ciapetti, L. Savarino, S. Stea, D. Cavedagna, a Di Leo, and a Pizzoferrato, “Adhesive protein expression on endothelial cells after contact in vitro with polyethylene terephthalate coated with pyrolytic carbon.,” *Biomaterials*, vol. 16, no. 16, pp. 1223–7, Nov. 1995.

[42] B. E. Sumpio, J. T. Riley, and A. Dardik, “Cells in focus: endothelial cell,” *Int. J. Biochem. Cell Biol.*, vol. 34, no. 12, pp. 1508–12, Dec. 2002.

[43] A. Cecchettini, S. Rocchiccioli, C. Boccardi, and L. Citti, *Vascular smooth-muscle-cell activation: proteomics point of view.*, 1st ed., vol. 288. Elsevier Inc., 2011, pp. 43–99.

[44] V. H. Rao, V. Kansal, S. Stoupa, and D. K. Agrawal, “MMP-1 and MMP-9 regulate epidermal growth factor-dependent collagen loss in human carotid plaque smooth muscle cells.,” *Physiol. Rep.*, vol. 2, no. 2, p. e00224, Mar. 2014.

[45] G. M. Risinger, T. S. Hunt, D. L. Updike, E. C. Bullen, and E. W. Howard, “Matrix metalloproteinase-2 expression by vascular smooth muscle cells is mediated by both stimulatory and inhibitory signals in response to growth factors.,” *J. Biol. Chem.*, vol. 281, no. 36, pp. 25915–25, Sep. 2006.

[46] K. Kanda, T. Matsuda, and T. Oka, “Mechanical stress induced cellular orientation and phenotypic modulation of 3-D cultured smooth muscle cells,” *ASAIO J.*, 1993.

[47] D. Seliktar, R. a Black, R. P. Vito, and R. M. Nerem, “Dynamic mechanical conditioning of collagen-gel blood vessel constructs induces remodeling in vitro.,” *Ann. Biomed. Eng.*, vol. 28, no. 4, pp. 351–62, Apr. 2000.

[48] V. K. Lee, D. Y. Kim, H. Ngo, Y. Lee, L. Seo, S.-S. Yoo, P. a Vincent, and G. Dai, “Creating perfused functional vascular channels using 3D bio-printing technology.,” *Biomaterials*, vol. 35, no. 28, pp. 8092–8102, Jun. 2014.

[49] Y.-B. Lee, S. Polio, W. Lee, G. Dai, L. Menon, R. S. Carroll, and S.-S. Yoo, “Bio-printing of collagen and VEGF-releasing fibrin gel scaffolds for neural stem cell culture.,” *Exp. Neurol.*, vol. 223, no. 2, pp. 645–52, Jun. 2010.